Accepted Manuscript

Rhodamine-azobenzene based single molecular probe for multiple ions sensing: Cu2+, Al3+, Cr3+ and its imaging in human lymphocyte cells

Subhabrata Mabhai, Malay Dolai, Surya Kanta Dey, Anamika Dhara, Sujata Maiti Choudhury, Bhriguram Das, Satyajit Dey, Atanu Jana

PII:	S1386-1425(19)30437-8
DOI:	https://doi.org/10.1016/j.saa.2019.04.056
Reference:	SAA 17064
To appear in:	*Spectrochimica Acta Part A: Molecular and Biomolecular Spectroscopy*
Received date:	4 March 2019
Revised date:	18 April 2019
Accepted date:	19 April 2019

Please cite this article as: S. Mabhai, M. Dolai, S.K. Dey, et al., Rhodamine-azobenzene based single molecular probe for multiple ions sensing: Cu2+, Al3+, Cr3+ and its imaging in human lymphocyte cells, Spectrochimica Acta Part A: Molecular and Biomolecular Spectroscopy, https://doi.org/10.1016/j.saa.2019.04.056

Rhodamine-azobenzene based single molecular probe for multiple ions sensing: Cu^{2+}, Al^{3+}, Cr^{3+} and its imaging in human lymphocyte cells

Subhabrata Mabhai,[a] Malay Dolai,[b] Surya Kanta Dey,[c] Anamika Dhara,[d] Sujata Maiti Choudhury, [c] Bhriguram Das,[e] Satyajit Dey,*[,e] Atanu Jana*[,f]

[a]Department of Chemistry, Mahishadal Raj College, East Midnapore, Mahishadal, West Bengal, Pin No. 721628, India.

[b]Department of Chemistry, Prabhat Kumar College, Contai, Purba Medinipur 721401, India.

[c]Department of Human Physiology with Community Health; Vidyasagar University, Rangamati, Medinipur, West Bengal, Pin No. 721102, India.

[d]Department of Chemistry, Jadavpur University, Raja S. C. Mallick Road, Kolkata 700032, India.

[e]Department of Chemistry, Tamralipta Mahavidyalaya, East Midnapore, West Bengal, Pin No. 721636, India. E-mail: *satyajitdeyoc@gmail.com*

[f]Center for Superfunctional Materials, Department of Chemistry, School of Natural Science, Ulsan National Institute of Science and Technology (UNIST), Ulsan 44919, South Korea
E-mail: *atanujanaic@gmail.com*

Abstract

A photoinduced electron transfer (PET) and chelation enhanced fluorescence (CHEF) regulated rhodamine-azobenzene chemosensor (**L**) was synthesized for chemoselective detection of Al^{3+}, Cr^{3+}, and Cu^{2+} by UV-Visible absorption study whereas Al^{3+} and Cr^{3+} by fluorimetric study in EtOH-H_2O solvent. **L** showed a clear fluorescence emission enhancement of 21 and 16 fold upon addition of Al^{3+} and Cr^{3+} due to the 1:1 host-guest complexation, respectively. This is first report on rhodamine-azobenzene based Cr^{3+} chemosensor. The complex formation, restricted imine isomerization, inhibition of PET (photo-induced electron transfer) process with the concomitant opening of the spirolactam ring induced a turn-on fluorescence response. The higher binding constants $6.7 \times 10^3\ M^{-1}$ and $3.8\times 10^3\ M^{-1}$ for Al^{3+} and Cr^{3+}, respectively and lower detection limits 1×10^{-6} M and 2×10^{-6} M for Al^{3+} and Cr^{3+}, respectively in a buffered solution with high reversible nature describes the potential of **L** as an effective tool for detecting Al^{3+} and Cr^{3+} in a biological system with higher intracellular resolution. Finally, **L** was used to map the intracellular concentration of

Al^{3+} and Cr^{3+} in human lymphocyte cells (HLCs) at physiological pH very effectively. Altogether, our findings will pave the way for designing new chemosensors for multiple analytes and those chemosensors will be effective for cell imaging study.

1. Introduction

Environmental pollution caused by the high concentration of heavy metals in sewage remains a global challenging problem. Heavy metal ions like Cu^{2+}, Al^{3+}, and Cr^{3+} provide essential indispensable nutrients for life when taken in regulated amount, but their uncontrolled or overexposure generates acute biological and physiological disorder [1–3]. Cu^{2+}, a cofactor of various enzymes like cytochrome co-oxidase, tyrosinase, and superoxide dismutase, plays a significant role in a physiological system such as iron regulation [4–6]. It turns as a toxic element when taken in excess of recommended amounts of 1.3 ppm (~20 μM) in drinking water and generated oxidative stress neuro degenerative diseases such as Alzheimer's disease, Wilson's disease, Menke's disease, gastro intestinal lipid metabolism disorders [7]. The toxic carcinogenic Cr^{6+} is converted to Cr^{3+} by bacterial reduction and bind nonspecifically with DNA to damage the intracellular activity like DNA replication and transcription [8]. Although Cr^{3+} is physiologically less harmful as compared to Cr^{4+} and Cr^{6+}, its deficiency increases the risk of diabetes, cardiovascular disease, and cancer [9]. Extensive use of other metal ion such as aluminum in modern life increases the risk of aluminum toxicity which bring calcium metabolism disorder, interferes the concentration of iron in the blood causing Osteomalacia, microcytic hypochromic anemia. Unregulated intake of aluminum cause encephalopathy, myopathy, dementia, Guamanian amyotrophic lateral sclerosis, Parkinson's disease, and Alzheimer's disease [10]. Therefore, a new challenging field is emerged for developing artificial chemosensor capable of recognizing the environmentally and physiologically important analytes in a rapid, inexpensive and sensitive way [11]. Due to high selectivity, sensitivity and easy operational use over other methods, colorimetric and fluorometric probes become the first choice for practical applications [12]. Meanwhile, the idea of designing a new cost-effective molecular probe which binds more than one analyte using a single detection method or an array of detection methods gain the importance over one-to-one normal sensors [13–15]. To date, in comparison to diamagnetic Al^{3+}, there are very few 'Switch-On' sensors reported for paramagnetic Cu^{2+} (d^9) and Cr^{3+}(d^3) because of their fluorescence quenching property [16]. Higher photostability and longer absorption-emission wavelength along with the ability to trigger a dramatic change in colour

by the opening of the non-fluoroscent closed shell to zwitterionic fluorescent spirolactam form make Rhodamine derivatives very reliable platform for constructing Off-On fluorescence sensor [17,18].

In this work, we have designed and synthesized a new (E)-2-hydroxy-3-methoxy-4-((4-nitrophenyl)diazenyl)benzaldehyde-appended rhodamine hydrazone derivative (**L**) in a mixed solvent as a single chemosensor for sensing multiple analytes such as Cu^{2+}, Al^{3+} and Cr^{3+}. The outline of the synthesis is depicted in **Scheme 1**. The sensor **L** exhibits the 'Turn-On' property via the chelation-enhanced fluorescence (CHEF) process [19] and inhibited PET which was supported by the different photophysical process. We have constructed INHIBIT molecular Logic gate using the sensing properties. The experimental findings are well-correlated with theoretical results using density functional theory calculations. In addition, **L** was successfully applied in the imaging of Al^{3+} and Cr^{3+} in human lymphocyte cells (HLCs).

2. Experimental Section

2.1 Materials and instruments

3-Ethoxysalicylaldehyde (99 %), p-nitro aniline (97 %), Rhodamine B (99.0 %) from Sigma-Aldrich, high-purity HEPES (99.0%), Na_2EDTA(98.0%), perchlorates and nitrate salts of the different metal cations (Ba^{2+}, Ca^{2+}, Cd^{2+}, Co^{2+}, Cu^{2+}, Cr^{3+}, Al^{3+}, Mn^{2+}, Fe^{3+}, Zn^{2+}, Ni^{2+}, Pd^{2+}, Mg^{2+}, Pb^{2+}, Na^{+}, Hg^{2+}) and all solvents were purchased from Merck (India) Ltd and were used as received without further purifications. All spectroscopic data were recorded using HPLC grade solvent. UV-Vis absorption study was performed with Evolution-201 spectrometer and XENO Flash (PTI) fluorescence spectrophotometer with quartz cuvette (path length = 1 cm) was utilized to record the emission spectra with the excitation wavelength 520 nm for both ligand and complex at room temperature. ^{1}H NMR spectra and ^{13}C NMR spectra were recorded on Brucker 400 MHz instruments using TMS as an internal standard. Chemical shifts (δ) were reported in ppm units and ^{1}H–^{1}H coupling constants in Hz. IR spectra (KBr pellet, 400–4000 cm^{-1}) were recorded on a Perkin-Elmer infrared spectrophotometer (Model: 883). Elemental analysis for carbon, hydrogen, and nitrogen was performed with Perkin Elmer 2400 CHN analyzer. Electrospray ionization MS (ESI-MS) on Qtof Micro YA263 mass spectrometer. Fluorescence Quantum Yield was calculated using Fluorescein an optically matching standard (Φr = 0.79). HORIBA Jobin Yvon Fluorocube-01-NL fluorescence lifetime spectrometer was used to record the time Correlated Single Photon

Counting (TCSPC) data. Gaussian software was used to have DFT data. Cell imaging was carried out with Fluorescence microscope (LEICA DFC295, Germany).

2.2 Isolation and culture of human lymphocyte cell (HLCs)

5 ml of blood samples were collected from healthy young volunteers according to the method of Hudson and Hay [20] about 4 ml of blood were layered onto the same amount of histopaque 1077 (Sigma-Aldrich Co. LLC, US) and centrifuged at 2000 rpm for 30 min at room temperature. To a centrifuge tube, the upper lymphocytes monolayer was transferred and washed three times in phosphate buffer solution (pH 7.4). The human lymphocyte cells (HLCs) were cultured by resuspending in RPMI medium supplemented with 10 % FBS and incubated for 24 h at 37 °C in a 95 % humidified and 5 % CO_2 atmosphere in a CO_2 incubator and used for the experimentation.

2.3 Cell cytotoxicity study

In order to measure the cytotoxicity of the ligand, yellow colored tetrazolium salt 3-(4, 5-dimethylthiazol-2-yl)-2S-diphenyltetrazolium bromide (MTT) assay was executed in human lymphocyte cells (HLCs) according to standard procedure [21]. In brief, overnight culture of HLCs were seeded in 96-well plates at a density of 1×10^6 cells per well in 100 µL of culture medium and incubated with a series of concentrations of **L** (5, 10, 20, 50 and 100 µM) at 37 °C in a 5 % CO_2 atmosphere for 24 h. After the removal of the culture medium, cells were washed by PBS (pH 7.4). 10 µl of MTT solution (1mg mL^{-1}) in PBS was added in each well and cell were again incubated for 3h at 37 °C. After the incubation, 0.1 % DMSO was added to each well. The absorbance of the intracellular formazan crystal (blue-violet) was measured at the wavelength of 540 nm by ELISA ANALYSER (Bio-Rad, Model 680). The cell viability was quantified as the optical density ratio of the ligand treated group to HLC-control. Values are mean (M) ± standard error of mean (SEM) of three independent experiments.

$$\% \text{ cell viabilty} = (\text{OD of the sample}) / (\text{OD of control}) \times 100$$

The cell cytotoxicity was calculated using the following formula:

$$\% \text{ cell cytotoxicity} = 100\ \% - \% \text{ cell viability}$$

2.4 Computational method

DFT study is an important tool to obtain better insights into the geometry, electronic structure, and optical properties of these systems. Ground state electronic structure calculations in gas phase of both the complexes have been carried out using DFT [22] method associated with the conductor-like polarizable continuum model (CPCM) [23–25]. Becke's hybrid function [26] with the Lee-Yang-Parr (LYP) correlation function [27] was used through the study. The geometry of the ligand and complex was fully optimized without any symmetry constraints. On the basis of the optimized ground state geometry, the absorption spectral properties in ethanol (EtOH) media were calculated by time-dependent density functional theory (TDDFT) [28–30] approach associated with the conductor-like polarizable continuum model (CPCM). We computed the lowest 40 singlet – singlet transition and results of the TD calculations were qualitatively very similar. The TDDFT approach had been demonstrated to be reliable for calculating the spectral properties of many transition metal complexes [31–33]**.** Due to the presence of electronic correlation in the TDDFT (B_3LYP) method, it yields more accurate electronic excitation energies. Hence TDDFT had been shown to provide a reasonable spectral feature for our complex of the investigation.

We have run the Gaussian for geometry optimization of both the complexes in ground state with 6-31G under B_3LYP. All the calculations were performed with the Gaussian 09W software package [34]. GaussSum 2.1 program [35] was used to calculate the molecular orbital contributions from groups or atoms.

2.5 Fluorescence lifetime measurements

Fluorescence lifetimes were measured by the method of Time-Correlated Single-Photon Counting (TCSPC) using a HORIBA JobinYvon Fluorocube-01-NL fluorescence lifetime spectrometer. The sample was excited using a laser diode at 450 nm and the signals were collected at the magic angle of 54.7 ° to eliminate any considerable contribution from fluorescence anisotropy decay [36]. The typical time resolution of our experimental setup is ~ 100 ps. The decays were deconvoluted using DAS-6 decay analysis software. The acceptability of the fits was judged by χ^2 criteria and visual inspection of the residuals of the fitted function to the data. Mean (average) fluorescence lifetimes were calculated using the following equation [37,38].

$$\tau_{av} = \frac{\sum \alpha_i \tau_i^2}{\sum \alpha_i \tau_i}$$

in which α_i is the pre-exponential factor corresponding to the ith decay time constant, τ_i.

2.6 Synthesis of Rhodamine B hydrazide:

Rhodamine B hydrazide was synthesized according to previously reported method [39].

2.7 Synthesis of 3-ethoxy-2-hydroxy-4-((4-nitrophenyl) diazenyl) benzaldehyde

The diazo compound was synthesized according to the literature procedure [40]. A clear green solution of p-nitroaniline (0.414 g, 3 mmol) in HCl (30 %, 6 ml) was prepared in between 0-5 °C by keeping the beaker on ice-salt bath with constant stirring. Colour of the solution changed from green to pale yellow during dropwise addition of cold aqueous $NaNO_2$ (0.207 g, 3 mmol). This diazotized solution was added to the alkaline solution of 3-ethoxy salicylaldehyde (0.5 g, 3 mmol) in water (20 ml) containing NaOH (0.12 g, 3 mmol) and (0.17 g, 1.63 mmol) at 5 °C. After overnight stirring of the resulting solution at room temperature a dark brown cake was produced, and it was filtered using Whatman-41. The dark-brown residue was reslurried after repeating washing by 10 % NaCl. The solution made slightly acidic (pH 4-5) by adding 2-3 drops of conc. HCl. Thereafter the yellow colour dye was dried by keeping in a vacuum desiccator and purity was confirmed by chromatography. The yield of the product was 85 %. ^{1}H NMR: [**Fig. S1, ESI**] [400 MHz, DMSO-*d6*, δ (ppm)] δ10.32 (1H, s, Ar-C**H**O), 8.35-8.33 (d, 2H, *J* = 8 Hz, Ar-**H**) 7.98-7.95 (d, 2H, J = 12 Hz, Ar-**H**) 7.87 (s, 1H, Ar-**H**) 7.62 (s, 1H, Ar-**H**) 4.18-4.13 (8H, q, *J* = 12Hz,-OC**H**$_2$) 1.38-1.35 (3H,t, *J* = 8Hz,-OCH$_2$C**H**$_3$). Melting point (M.P.) 184 °C.

2.8 Synthesis of chemosensor L

An easy and convenient one-step condensation method was applied to the synthesis of **L** from Rhodamine B hydrazide and aldehyde precursor (**Scheme 1**). Rhodamine B hydrazide (0.460 g, 1.008 mmol) and 2-ethoxy-6-methyl-4-((4-nitrophenyl)diazenyl)phenol (0.319 g, 1.008 mmol) were dissolved in dry EtOH (20 ml) by stirring at room temp. The resulting solution was refluxed for 6-hrs with constant monitoring by thin layer chromatography (TLC). At the end of the reaction, the volume of the reaction mixture is reduced to 1/3 of its original volume so that a deep red colored solid appeared. The deep red colored solid was separated by simple filtration and washed repeatedly by cold EtOH-Ether (1:1 ratio) after cooling the reaction at room temperature. Yield ~ 85 %. M.P. 220 °C

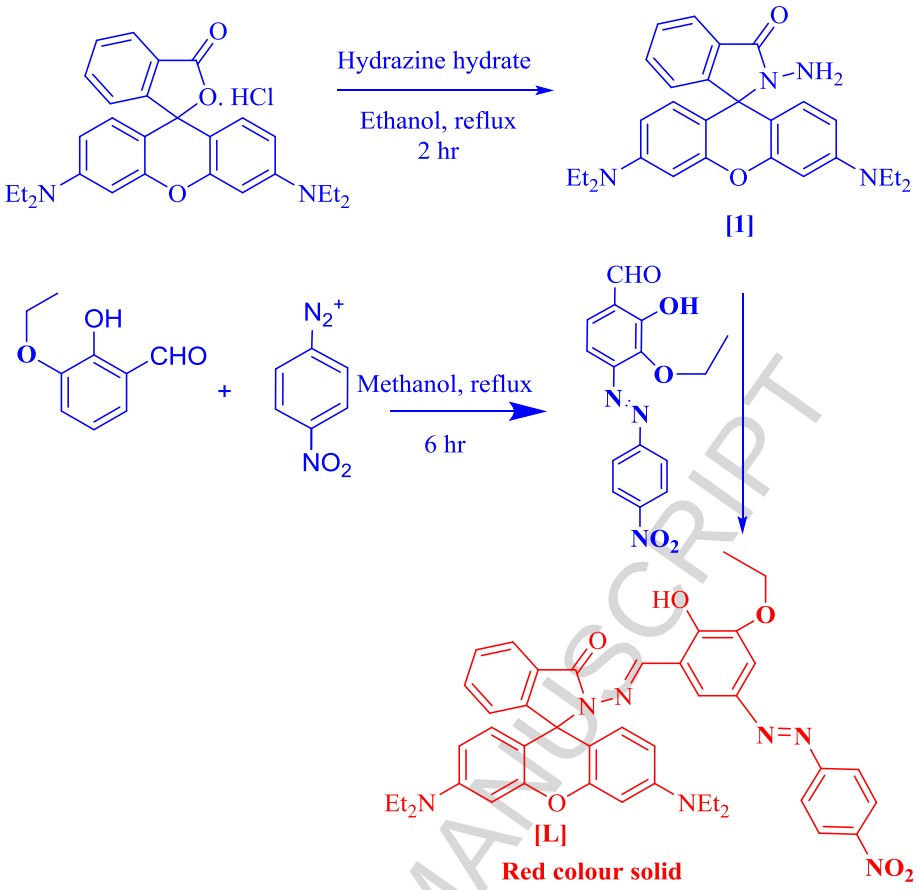

Scheme 1. Synthesis of chemosensor **L**

^{1}H NMR [**Fig. S2, ESI**] [400 MHz, DMSO-*d6*, δ (ppm)] δ10.92 (1H, s, -O**H**), 9.16 (1H, s, –C**H**=N), 8.39-8.37 (2H, d, *J* = 8 Hz), 8.00-7.98 (2H, d, *J* = 8Hz), 7.94-7.92 (1H, d, *J* = 8 Hz), 7.76 (1H, s), 7.63-7.56 (2H, m), 7.43 (1H, s), 7.11-7.10 (1H, d, *J*=4Hz), 6.46-6.44 (4H, m), 6.37-6.34 (2H, dd, *J* = 12 & 8Hz), 4.11-4.10 (2H,q, *J* = 8 Hz), 2.50-2.48 (8H, q, *J* = 4Hz,-OC**H**$_2$), 1.35-1.31 (3H,t, *J* = 8Hz,-OCH$_2$C**H**$_3$), 1.07-1.03 (12H, t, *J* = 8Hz,-NCH$_2$C**H**$_3$)**.** ^{13}C NMR [**Fig. S3, ESI**] [125 MHz CDCl3, δ (ppm)] :12.90, 19.53,14.92, 44.15, 64.81, 66.03, 97.90, 105.23,108.70,122.88,123.65, 124.13, 124.36, 125.40,125.53, 127.66, 128.11, 128.41, 133.88, 134.65, 144.73,145.31,146.08, 149.07,152.04,153.14,159.70,164.32**.** Elemental analysis (calcd. %) for $C_{43}H_{43}N_7O_6$: C, 68.51; H, 5.75; N, 13.01; O, 12.73; found (%): C, 68.48; H, 5.78; N, 13.03; O, 12.70. ESI-MS: [**Fig. S4, ESI**] m/z calculated for $C_{43}H_{43}N_7O_6$ $[M+H]^+$:754.33, found 754.66.

2.9 Synthesis of L-Al^{3+} and L-Cr^{3+}Complex

$Al(NO_3)_3.9H_2O$ (0.19 g, 0.506 mmol) and $CrCl_3$ (0.080 g, 0.506 mmol) were added to the two separate R.B. each containing (0.381 g, 0.506 mmol) of **L** in acetonitrile. The solution was

filtered after overnight stirring at room temperature. The deep maroon colored solid filtrate appeared in both case after several time washing with MeOH kept in vacuum for drying.[1]H NMR [**Fig. S5, ESI**] [400 MHz, DMSO-*d6*, δ (ppm)] δ 9.44 (1H, s, –CH=N), 8.41-8.39 (2H, d, *J* = 8 Hz), 8.00-7.93 (3H, M), 7.78 (1H, s), 7.62-7.60 (2H, m), 7.44 (1H, s), 7.12-7.10 (1H, d, *J* = 8 Hz), 6.46-6.44 (4H, m), 6.37-6.32 (2H, m,), 4.11-4.09 (2H,q, *J* = 4 Hz), 2.51-2.49 (8H, q, *J* = 4Hz,-OC**H**$_2$), 1.36-1.33 (3H,t, *J* = 8Hz,-OCH$_2$C**H**$_3$), 1.08-1.04 (12H, t, *J* = 8Hz,-NCH$_2$C**H**$_3$). ^{13}C NMR [**Fig. S6, ESI**] [125 MHz CDCl3, δ (ppm)] : 12.86, 14.06, 14.86, 44.15, 64.82, 97.90, 108.74, 120.94, 120.91, 122.24, 123.64, 124.02, 125.51, 128.10, 128.71, 129.44, 129.97, 132.67, 134.68, 144.72, 145.22, 148.45, 148.57, 151.95, 153.11, 157.27, 157.87, 158.28, 162.07.^{13}C NMR [**Fig. S7, ESI**] [125 MHz CDCl3, δ (ppm)] :12.94, 15.31, 39.90, 40.06, 40.22, 40.39, 40.55, 40.72, 40.88, 44.20, 64.83, 97.87, 104.70, 105.13, 108.70, 120.06, 120.78, 1213.74, 124.34, 125.60, 128.09, 128.69, 131.46, 145.22, 145.25, 14.17, 148.41, 148.56, 149.06, 151.93, 153.11, 164.40.ESI-MS: **[Fig.S8, S9, ESI]** m/z calculated for $C_{43}H_{43}N_7O_6$ [L+Al+NO_3+H+]+ : 841.1625, found 841.1625 and for $C_{43}H_{43}N_7O_6$ [L+Cr+] : 804.51 found 804.51.

2.10 Association constant

The association constant value (*Ka*) was determined from absorption data using the following Benesi–Hildebrand (B–H) equations [41].

$$\frac{1}{(A-A_0)} = \frac{1}{[K(A_{max}-A_0)C]} + \frac{1}{(A_{max}-A_0)}$$

where $\mathbf{A_0}$ is the absorbance maxima of sensor **L**, **A** is the observed absorbance at that particular wavelength at different concentration of the metal ion [C], A_{max} is the maximum absorbance value at λ_{max} = 582 nm and 581 nm for Al^{3+} and Cr^{3+}, respectively during titration with varying [C], K is the association constant and was determined from the ratio of slope and intercept of the linear plot, and [C] is the concentration of the $\mathbf{M^{n+}}$ ion added during titration studies.

The binding constant is determined from fluorescence intensity data using Benesi–Hildebrand equation:

$$\frac{1}{(I-I_0)} = \frac{1}{(I_1-I_0)} + \frac{1}{(I_1-I_0)k[M^{n+}]^m}$$

where $[M^{n+}]$ is the metal ion concentration, $\mathbf{I_0}$, **I** and $\mathbf{I_1}$ indicate emission intensities in the absence of, at intermediate and at infinite concentrations of metal ions, respectively. An

aqueous stock solution of M^{n+} in H_2O with an exact concentration of 1×10^{-3} mol L^{-1}, in an aqueous HEPES buffer (pH 7.2) and an effective concentration of 2×10^{-5} mol L^{-1} ligand solution was prepared in the EtOH-H_2O medium at pH 7.2 for this purpose.

A linear relationship between **$1/(A-A_0)$ vs. $1/[M^{n+}]$** plot indicates 1:1 binding stoichiometry and the binding constant calculated to be 6.7435×10^3 M^{-1}, 3.8×10^3 M^{-1} respectively for Al^{3+} and Cr^{3+} and 5.685×10^3 M^{-1} for Cu^{2+} (**Fig. S10, S11, S12 ESI**).

2.11 Procedure for metal ion sensing

A stock solution of the sensor **L** was prepared with concentration 1×10^{-3} in Ethanol-aqueous HEPES buffer (5μM, pH 7.2, 9:1, v/v) for both spectroscopic studies. Metal solution of different conc. (C = 1×10^{-3}, C = 1×10^{-2}) were prepared from Ethanol-de-ionized water. Absorbance and fluorometric selectivity were examined by taking 20 μL of the stock solution in 2 ml ethanol in a quartz cuvette (path length, 1 cm) maintaining the final conc.10×10^{-6} M along with 50μL (C = 1×10^{-2}) metal solution. Titration experiment was carried out by the gradual addition of metal ion (C = 1×10^{-3}) to sensor solution.

2.12 Fluorescence Quantum Yield

Fluorescein an optically matching standard (Φr = 0.79) was used in spectroscopic grade EtOH to determine the Fluorescence Quantum Yield by the following Equation [42].

$$\Phi_s = \Phi_r\left(\frac{A_r F_s}{A_s F_r}\right)\left(\frac{\eta_s^{\,2}}{\eta_r^{\,2}}\right)$$

Where *As* and *Ar* are the absorbance of the sample and reference solutions, respectively, at the same excitation wavelength, *Fs* and *Fr* are the corresponding relative integrated fluorescence intensities, and η is the refractive index of the solvents. The Quantum Yield of ligand Φ = 2.94 %, changes to 11 fold Φ = 32.6 % for Al^{3+} and 3.61 fold Φ = 10.6 % for Cr^{3+}.

2.13 Binding ratio measurements (Job's plot)

Job's plot measurement was made from UV-Vis titration. Receptor solution was taken in 10 vials at regular intervals starting from 20 μL to 2 μL. whereas metal solution was injected into it in reverse order at the same regular interval. The total solution volume of each vial is fixed to 2mL. Absorption data was recorded out at room temperature after shaking the vials for 2 minutes [43].

3. Results and discussion

3.1 Selectivity studies

Selectivity of **L** is ascertained spectrometrically by taking 25 equivalent of several competitive metal ions (Ba^{2+}, Ca^{2+}, Cd^{2+}, Co^{2+}, Cu^{2+}, Cr^{3+}, Al^{3+}, Mn^{2+}, Fe^{3+}, Zn^{2+}, Ni^{2+}, Pd^{2+}, Mg^{2+}, Pb^{2+},Na^{+}, Hg^{2+}) in a solution containing 20 µL **L** in 2 mL EtOH-H_2O (9:1,v/v, 5µM HEPES pH 7.2) solvent. The result exhibited that Al^{3+}, Cr^{3+} and Cu^{2+} exhibit sharp change in absorbance whereas Al^{3+} and Cr^{3+} show distinct change in PL intensity with respect to other metal ions. Al^{3+}, Cr^{3+}, and Cu^{2+} altered the absorbance spectral line with the appearance of three bands at λ_{max} = 551, 554, and 557 nm, respectively under the identical condition. Under this optimal condition (i.e.; pH = 7.2) **L** changes its fluorescence spectral line in presence of $Cr^{3+}$and Al^{3+} at 581 nm & 582 nm, respectively. The superior dual fluorometric selectivity of **L** was experienced in the naked eye after 366 nm radiation of UV light where the color of the **L** changed immediately from colourless to deep pink after the addition of Al^{3+} and Cr^{3+}. Such interesting findings motivate our groups to explore the **L** as a single probe for dual metal sensing by fluorometric method. Though in ambient light, **L** shows colorimetric distinction with Ba^{2+}, Ca^{2+}, Co^{2+} (dark yellow), $Fe^{3+}$and Pd^{2+} along with the Al^{3+}, Cr^{3+}, and Cu^{2+} metal ions (**Fig. 1**), but in UV-Visible absorption study, our sensor shows a prominent change in absorbance only with three metal ions (Cu^{2+}, Al^{3+}, and Cr^{3+}) whereas $Cr^{3+}$and Al^{3+} are distinguished from other metal ions by PL study. Oxophilic, diamagnetic, hard acid Al^{3+} with its high ionic potential and low ionic radius provides strong binding energy with the hard base than other paramagnetic divalent and trivalent metal ions, and hence make them as a strong guest for **L** [43,44]. Again particularly intersystem crossing in excited singlet state by transferring electron from paramagnetic Cu^{2+} (d^9) to the Rhodamine-B fluorophore promotes the intersystem absorption phenomena making it a natural fluorescence quencher [45],[46].

3.2 Spectroscopic recognition.

3.2.1 UV-Visible absorption studies:

The extraordinary dual sensitivity by this newly designed rhodamine-based probe was investigated by UV-Vis and fluorescence method, using different metal solution in EtOH-H_2O (9:1 V/V) at optimized pH 7.2. The color of **L** changes upon addition of Ba^{2+}, Ca^{2+}, Co^{2+}, Fe^{3+}, and Pd^{2+} along with the Al^{3+}, Cr^{3+}, and Cu^{2+} metal ions but only Cr^{3+} and Al^{3+} exhibit pink color under UV light (366 nm) (**Fig. 1**). This optical discrimination was further justified during the quantitative recording of UV-Visible absorption spectra of several analytes *viz.* Na^{+}, K^{+}, Ba^{2+}, Ca^{2+}, Cd^{2+}, Co^{3+}, Cr^{3+}, Cu^{2+}, Fe^{3+}, Hg^{2+}, Mg^{2+}, Mn^{2+}, Ni^{2+}, Pb^{2+}, Pd^{2+}, Zn^{2+} and Al^{3+} in aforementioned ligand solution taken in a quartz tube containing 2 ml

EtOH-H_2O (9:1, v/v) pH = 7.2 using 5 µM HEPES buffer at 25 °C. Interestingly, as depicted in **Fig. 2,** UV-Visible spectral results revealed that among the all coexisting metal ions only Cu^{2+}, Al^{3+}, and Cr^{3+} alters the spectral line at λ_{max} = 551, 554 and 557 nm, respectively. To have a better quantitative appraisal of the reversible interaction of the sensor **L**, absorption spectral variation was carried out between sensor **L** with $M^{n+}$and resulting chelated complex with a more powerful hexadentate chelating agent Na_2EDTA. Gradual incremental addition of Al^{3+}, Cr^{3+}, and Cu^{2+}, to the fixed solution of sensor **L** (2 ml) in EtOH-H_2O (9:1, v/v) at pH = 7.2 a progressive increase of the absorption peak for the guest metals were observed along with deepening of pink color. After addition of 46 µM Al^{3+}, 36 µM Cr^{3+} and 50 µM Cu^{2+}, no further increment was observed at λ_{max} = 554, 557 and 551 nm, respectively, for Al^{3+}, Cr^{3+} and Cu^{2+}.

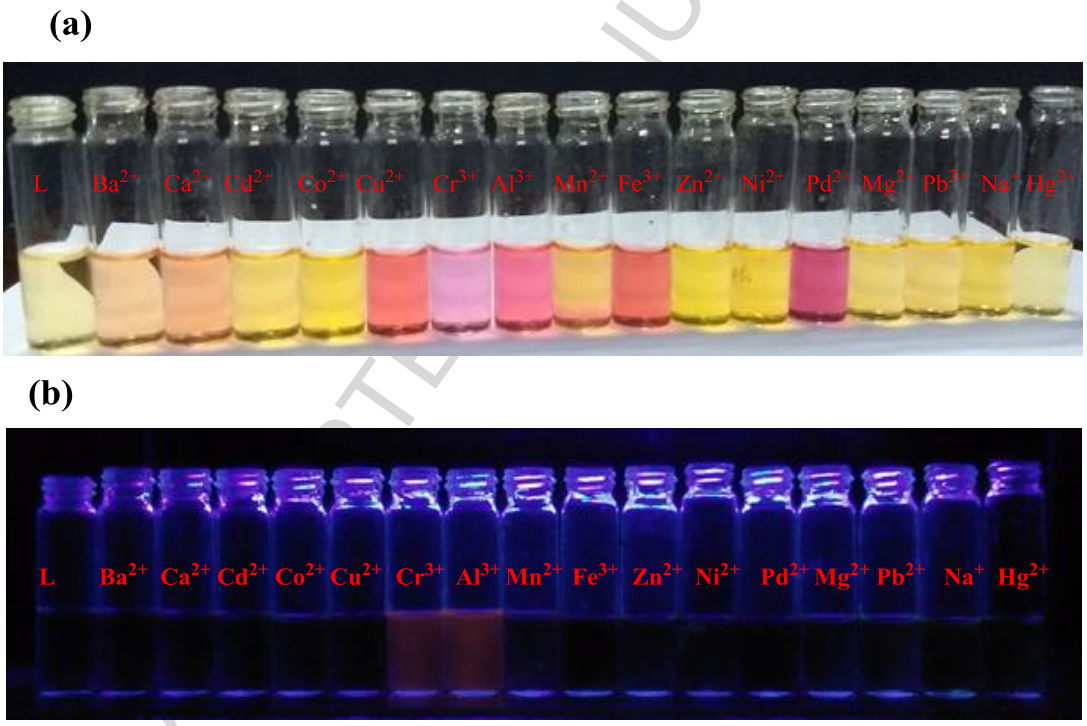

Fig. 1. Visual display of **L** plus metal ions: (a) under normal illumination (b) and demonstrating fluorescence under 365 nm illumination.

This indicates the chelating saturation of sensor **L** for guest metal ions due to the transformation of Rhodamine B from close spirolactam ring to stable metal-induced open conjugated xanthene form (**Fig. 3 (a-c))** [47]. However, complete bleaching of pink colour, as

well as the disappearance of aforementioned peaks (**Fig. 3 (d-f)**) by the incremental addition of Na_2EDTA, clearly indicates reversible binding nature of sensor ligand towards the guest cation. Association constant was calculated from absorbance vs. $[M^{n+}]$ curve by Benesi-Hildebrand linear curve fitting methods and was found to be $k_a = 6.7435\times10^3\ M^{-1}$, $3.8\times10^3 M^{-1}$, and $5.685\times10^3\ M^{-1}$, respectively, for Al^{3+}, $Cr^{3+,}$ and Cu^{2+}. (**Fig. S10, S11, S12 ESI**).The calculated LOD value $1.07x10^{-6}$ M, $2.02\ x10^{-6}$ M, 1.6×10^{-6} M for Al^{3+}, Cr^{3+} and Cu^{2+} based on UV-Visible absorption data by 3σ method [48] also satisfies the limit of drinking water for both Al^{3+} and Cr^{3+} (**Fig. S13, S14, S15 ESI**).

As our purpose is to establish the designed sensor as an effective fluorescent probe so we are not interested to explore the fluorometric sensing property of Cu^{2+} as it does not obliterate the fluorescent spectral nature of the sensor **L**.The selectivity tuning of **L** towards Al^{3+} and Cr^{3+} was explored by the fluorometric method.

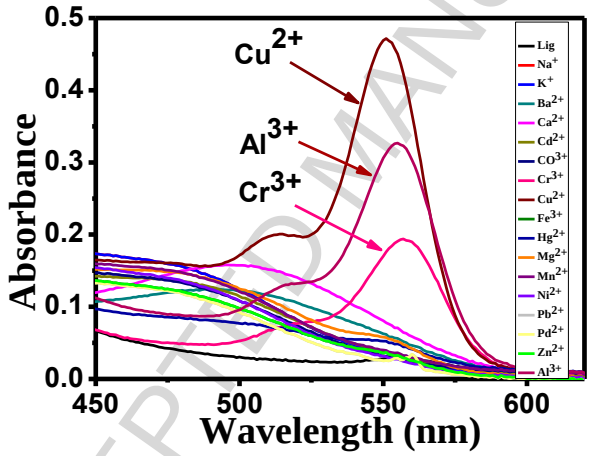

Fig. 2. Absorption spectral nature of Probe **L** upon addition of various metal ions (Na^+, K^+, Ba^{2+}, Ca^{2+}, Cd^{2+}, Co^{3+}, Cr^{3+}, Cu^{2+}, Fe^{3+}, Hg^{2+}, Mg^{2+}, Mn^{2+}, Ni^{2+}, Pb^{2+}, Pd^{2+}, Zn^{2+}, and Al^{3+}) 25 equiv. in EtOH-H_2O [9:1, v/v, 5 µM HEPES pH 7.2] at 25 °C

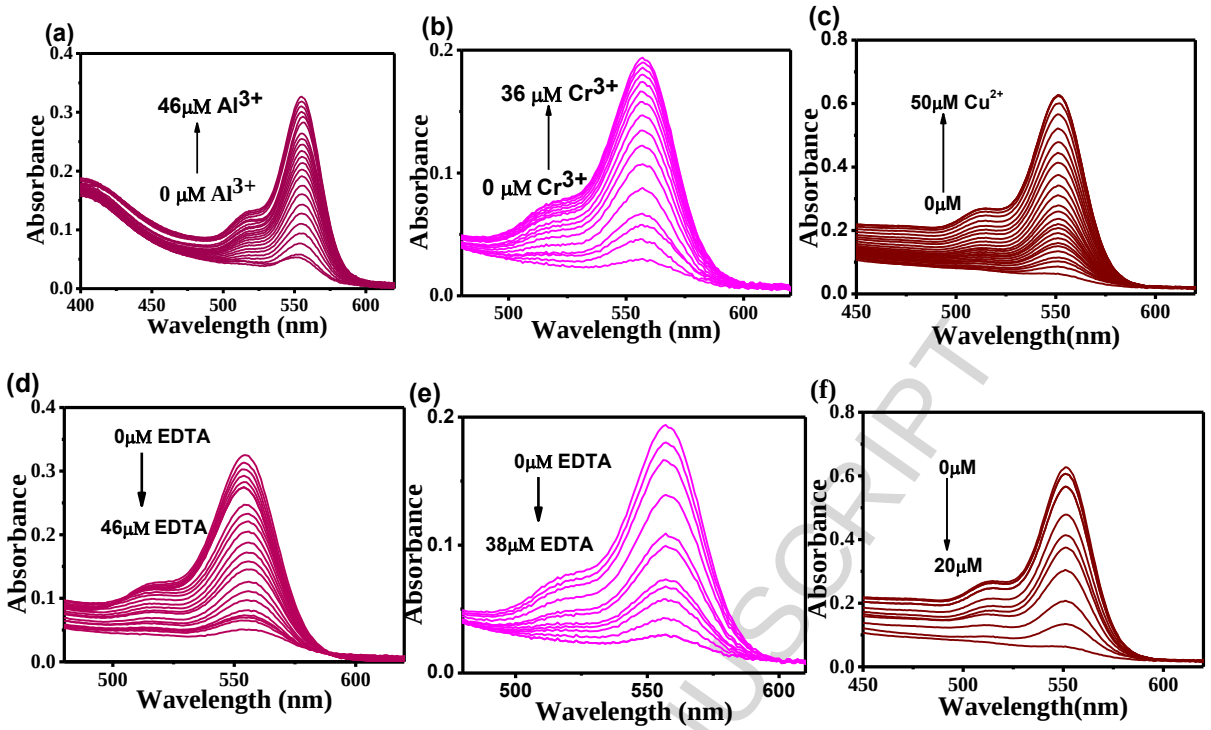

Fig. 3. UV-Vis absorption spectra of sensor Probe **L** (10μM) upon titration with (a) Al^{3+} (b) Cr^{3+} (c) Cu^{2+} (c =1.0×10^{-3} M) in EtOH-H_2O [9:1, v/v, 5μM HEPES pH 7.2]. Absorbance spectra of sensor (d) **L**-Al^{3+}, (e) **L**-Cr^{3+},and (f) **L**-Cu^{2+} complex upon incremental addition of EDTA

3.3 Fluorescence study

A better understanding of emissive behavior of sensor **L** is explored by choosing an appropriate solvent. The emissive behavior of **L**-Al^{3+} and **L**-Cr^{3+}in different solvents (EtOH, MeOH, CH_3CN, DMF, and DMSO) were tested with the findings that in both cases EtOH was the suitable solvent for the study of emissive property (**Fig. 4)**. The selectivity and sensitivity trait of **L** towards Al^{3+} and Cr^{3+} with respect to other alkali and alkaline earth metal analytes such as Na^+, K^+, Ba^{2+}, Ca^{2+}, Cd^{2+}, Co^{3+}, Cu^{2+}, Fe^{3+}, Hg^{2+}, Mg^{2+}, Mn^{2+}, Ni^{2+}, Pb^{2+}, Pd^{2+} and Zn^{2+} at pH = 7.2 using 5 μM HEPES buffer at 25 °C was also pursued by exciting the sensor solution above λ_{max} = 520 nm in optically matching 2 ml EtOH-H_2O (9:1, v/v) solution. Under the experimental condition, no noticeable emission peak for ligand was observed in the presence of alkali and alkaline earth metal ions except for a very weak absorption for Cu^{2+} was detected at λ_{max} = 574 nm and fascinatingly, enough under the same experimental condition, Al^{3+} and Cr^{3+} generate a remarkable fluorescence enhancement of 21

fold and 16 fold at λ_{max} = 582 nm and 581 nm, respectively (**Fig. 5**) as a result of metal-induced CHEF process and inhibition of PET process, when 25 eq. of different metal ions were added to the sensor solution.

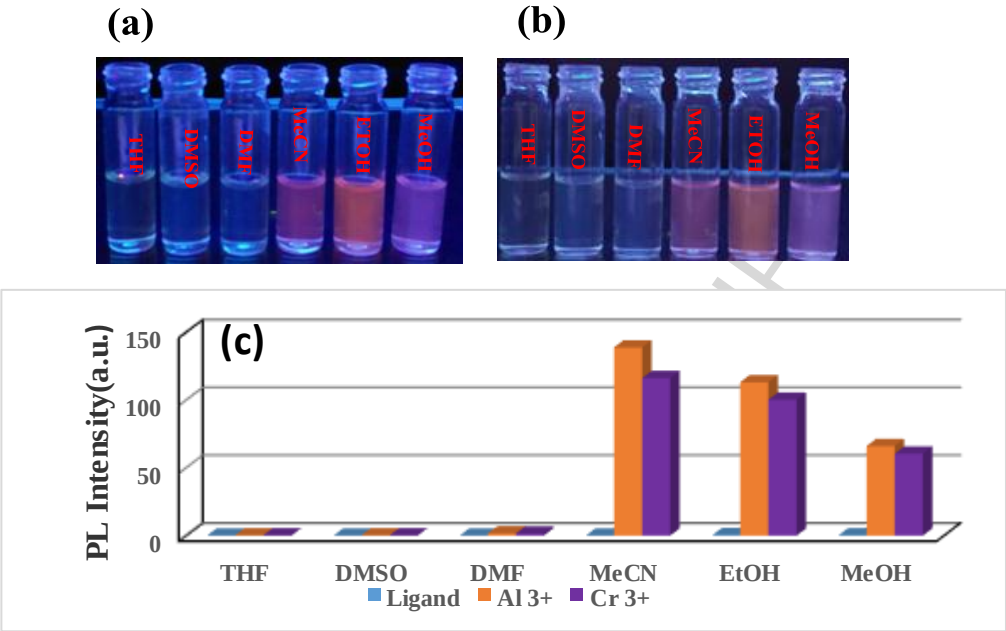

Fig. 4. Solvent effect on the emissive behavior of sensor **L** towards (a) $Al^{3+}$and (b) Cr^{3+} ions. Inset: Photographic image of the emissive pattern in the different solvent system under UV-cabinet (λ = 366 nm) (a) **L**-Al^{3+} (b) **L**-Cr^{3+}

The onset of Photo-induced electron transfer (PET) process by –C=N bond isomerization along with a donation of an electron from HOMO of Schiff base N and –OH of hydroxyl aldehyde to fluorophore LUMO is mainly responsible for 'Turn-Off' emissive behavior of the sensor [49]. Again the inhibition of isomerization and appropriate complexation in presence of specific guest and functional group attached to the fluorophore makes the PET process invalid and initiates the chelation-enhanced fluorescence process (CHEF) by transferring HOMO electron of the fluorophore to its LUMO arresting the previous electron transfer [50] (**Scheme 2)**. This strong 'Turn-On' selectivity of sensor **L** also observed when sensor solution treated separately with each of 25eq. Al^{3+} and Cr^{3+} under long-range UV lamp of (366 nm). The almost immediate transformation of colourless sensor solution to pink colour supports the 'Turn-On' property of the sensor.

To elucidate the reversible binding mode of sensor **L** fluorescence titration was performed with Al^{3+} and Cr^{3+}. Fluorescence intensity increases maximally up to λ_{max} = 582 nm and 581

nm with the gradual addition of 46 µM $Al^{3+}$and 36 µM of Cr^{3+} (**Fig. 6 (a-b)**) after which increment ceases down with a quantum yield (Φ = 11.08) for Al^{3+} and (Φ = 3.61) for Cr^{3+}, respectively. The fluorescence intensity decreases gradually almost by the similar manner with the incremental addition of Na_2EDTA **(Fig. 6 (c-d))** due to the removal of metal ions from the **L**-M^{3+} complex by the formation of strong chelate with EDTA. The lower quantum yield and lower emission intensity of Cr^{3+}in compared to $Al^{3+}$is attributed to the higher oxophilic nature higher CFSE value and hard acid character of Al^{3+}, which encourages the higher CHEF effect of the sensor for Al^{3+}.

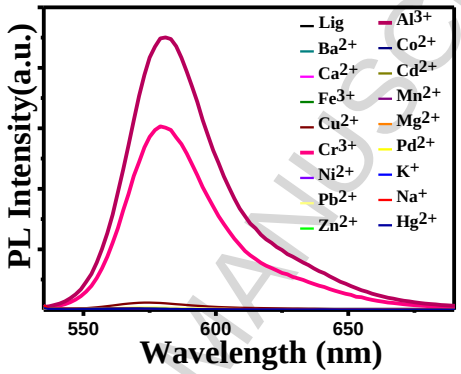

Fig. 5. Emission spectral nature of Probe **L** (10 µM) upon addition of various metal ions (10 equiv.) in EtOH-H_2O [9:1, v/v, 5 µM HEPES pH 7.2] at 25 °C

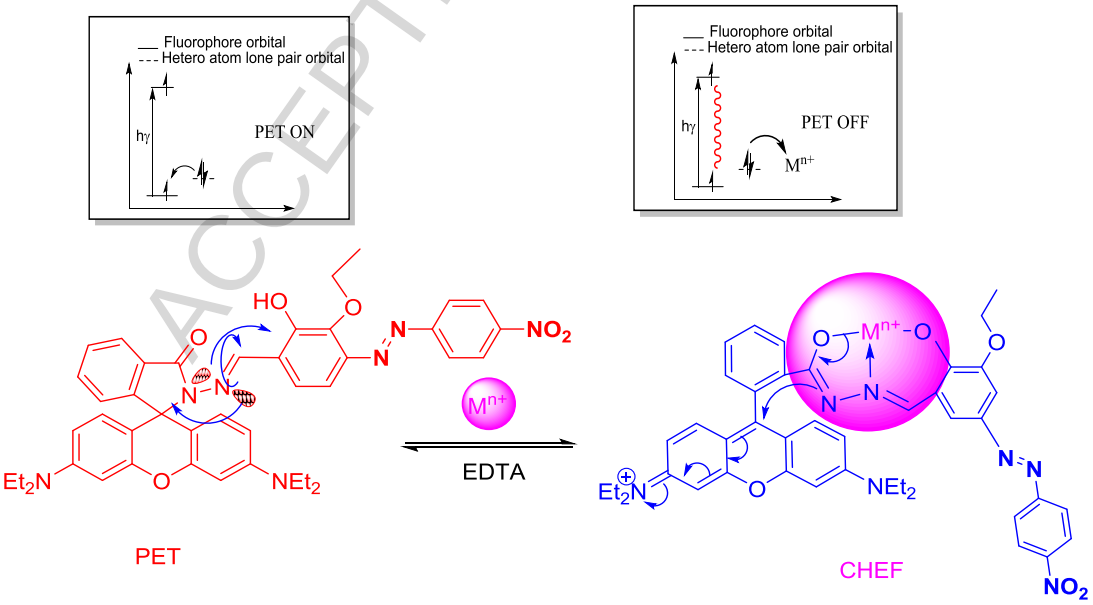

Scheme 2. Schematic Presentation Showing the Possible PET-CHEF mechanism for Al^{3+} and Cr^{3+}sensing.

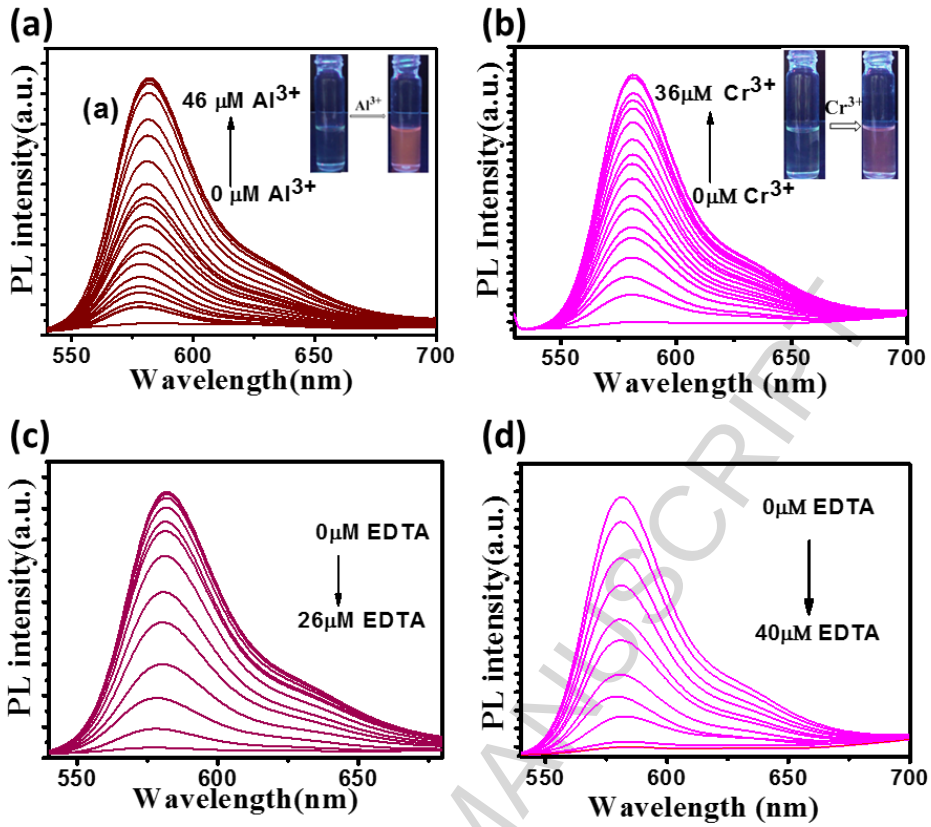

Fig. 6. Emission spectral change of the ligand **L** (10μM) upon incremental addition of (a) Al^{3+} and (b) Cr^{3+} in EtOH-H_2O [9:1, v/v, 5 μM HEPES pH 7.2] at 25 °C. Emission spectral change of the (c) **L**-Al^{3+} and (d) **L**-Cr^{3+} complex upon incremental addition of EDTA in EtOH-H_2O [9:1, v/v, 5 μM HEPES pH 7.2] at 25 °C.

3.4 Interference studies

For effective use of the probe, achieving high selectivity as a host for Al^{3+} and Cr^{3+} in presence of other potentially challenging metal cation is a very important index. In order to check the cross sensitivity, we do perform the selectivity of our probe for a wide range of cations along with Al^{3+} and Cr^{3+} in the EtOH-H_2O medium. Clearly, it is revealed from the graph that the emission intensity of the probe remains almost unchanged when 5 equivalents of other metal ions added to the buffer solution of the probe as that of Al^{3+} and Cr^{3+} **(Fig. 7)**. Surprisingly in both case after the addition of 10 equivalents of Cu^{2+} and Fe^{3+}, there was a rapid quenching of fluorescent intensity. Fe^{3+} quenches the intensity because of the stability of its half-filled (d^5) shell [51] and the onset of non-radiative decay caused by the electron transfer from redox active (d^9) Cu^{2+} to the excited fluorophore of rhodamine moiety is one of the probable reasons for fluorescence quenching.

Therefore, the dual metal experiment clearly evidenced that our probe can be used as a dual target recognizing agent in a single detection method.

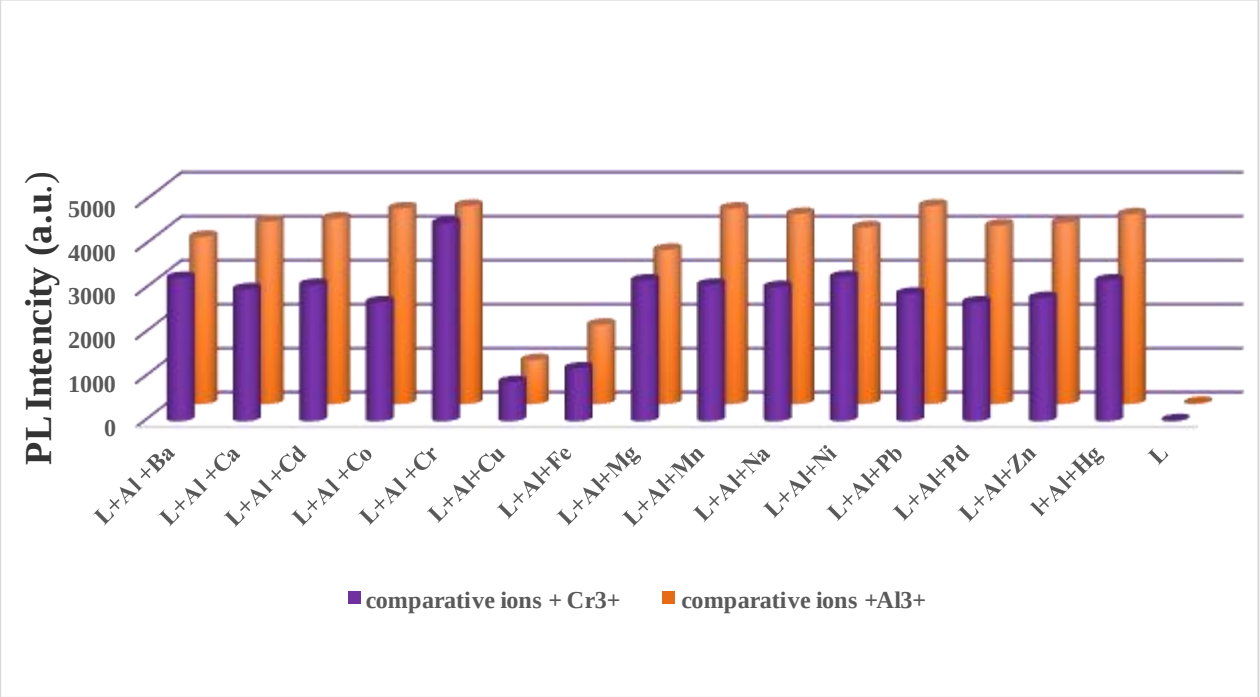

Fig. 7. Relative emission intensity of **L** after addition of 5 equivalents of competing for metal ions as that of Al^{3+}/$Cr^{3+}$to the solution of **L** in EtOH-H_2O [9:1, v/v, 5 µM HEPES pH 7.2] at 25 °C.

3.5 Reversibility

The practical usability of **L** depends mainly on its alternating enhancing and reviving mechanism. This reversibility is investigated to monitor the important changes in the biological system. Hexadentate chelating agent Na_2EDTA bleach the 'signal-on' absorption band of both Al^{3+} and Cr^{3+} through the process of demetallation from **L**-M^{n+} complex by regenerating the spirolactam ring. Our reversibility experiment well substantiates this theory. Addition of Na_2EDTA to the **L**-M^{n+} complex solution completely arrests the fluorescent by returning it to the 520 nm indicating the generation of metal-free ligand. Turned-on property of **L** is regained upon addition of either Al^{3+} or Cr^{3+}. This result is recreated after sequential several additions of metals and Na_2EDTA, which clearly indicates that the receptor reversibly recognized Al^{3+} and Cr^{3+} (**Fig. 8)**.

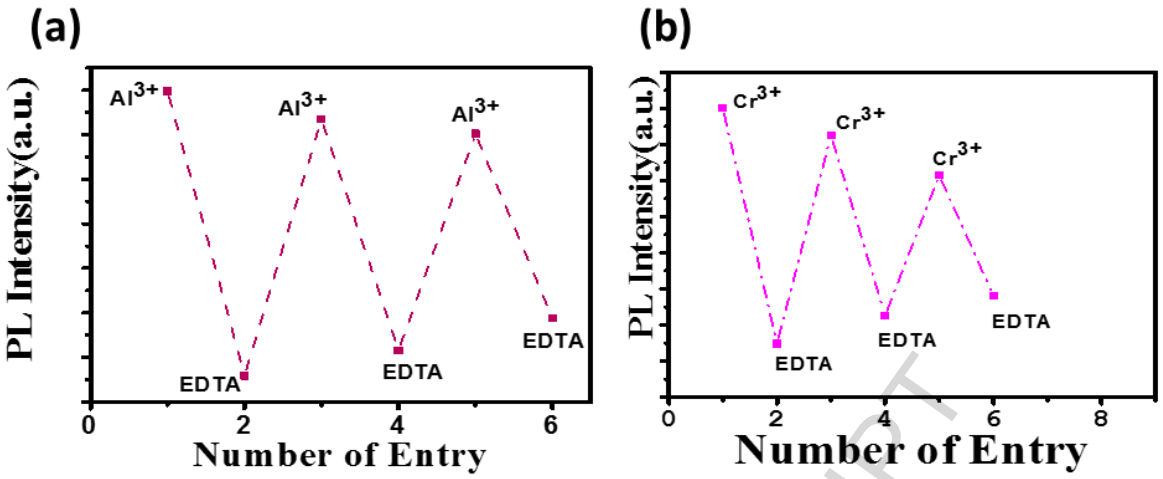

Fig. 8. Changes of emission intensity at 582 nm (λ_{ex} = 520 nm, 10 μM) in EtOH-H_2O (9:1, v/v at pH = 7.2 HEPES buffer) upon repetitive addition of (a) Al^{3+} (1.0 equiv.) and EDTA solution. (b) changes of emission intensity at 581 nm (λ_{ex} = 520 nm, 10μM) in EtOH-H_2O 9:1, v/v at pH = 7.2 HEPES buffer) upon repetitive addition of Cr^{3+} (1.0 equiv.) and EDTA solution.

3.6 pH study

The **L** can only be used effectively in a complex biological system if it can withstand in physiological pH without hydrolysis by the interfering proton. Although we have used HEPES buffer solution to arrest the hydrolysis of guest metal ion throughout the sensing process so as to eliminate any type of chance that may be caused by the participation of proton in incremental fluorescent luminescence, the pH study has been performed over a long-range of pH (2-12) in EtOH-H_2O (9:1 v/v) medium both in the presence and absence of metal ions [52]. At lower pH, the protonation induced spirolactam ring opening affects the gradual increment of fluorescence intensity of probe **L** irrespective of the inclusion of metal ions. However, in presence of metal ions, the probe **L** shows excellent fluorescent sensing ability which remains almost unaltered throughout the physiological range of pH. On another site, there is no observable emission for the probe **L** in absence of analytes within this physiological range as it remains in its spirolactam form in this pH (**Fig. 9)** [53]. This very conclusive study clearly negates any type of interference of the proton in physiological pH and indicates that the luminescence in the physiological pH is only due to **L**-M^{n+} binding

spirolactam ring opening. So clearly this novel sensor is a biocompatible one for detection of Al^{3+} and Cr^{3+}.

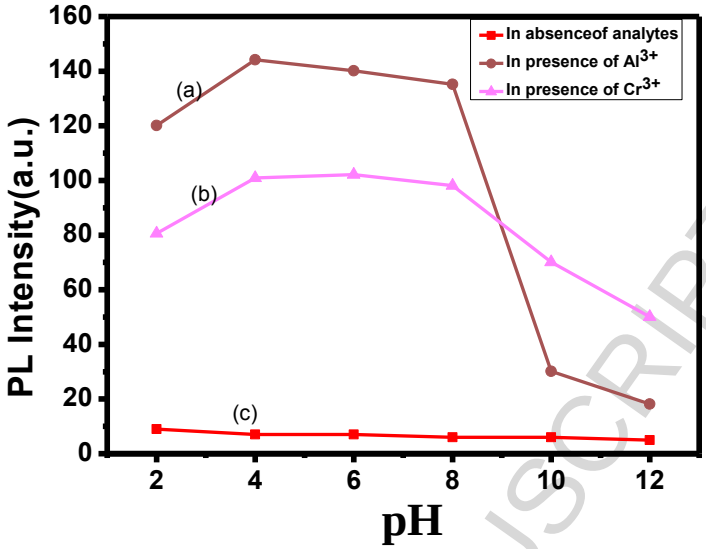

Fig. 9. Fluorosenseresponse of (a) **L**-Al^{3+} (brown line) at λ_{max} = 582 nm, (b) **L**- Cr^{3+} (pink line) at λ_{max} = 581 nm, and (c) **L** (red line) as a function of pH in EtOH-H_2O 9:1, v/v at pH = 7.2 HEPES buffer) at 25 °C at the excitation wavelength of 520 nm. The pH was adjusted using 1 M aqueous solutions of HCl.

3.7 Plausible mechanism

The conspicuous 'Turn-On' behaviour of **L** towards Al^{3+} and Cr^{3+} is a combination of the PET-CHEF process. The Turn Off fluorescent property which is possibly responsible for a lower quantum yield of **L** is due to PET process where lone pair from N center of spirolactam moves to the azobenzene moiety making the spirolactam tautomer colorless [54]. On the other hand, colourless non-fluorescent to the pink fluorescent makeover of **L** is an obvious result of the binding-induced spirolactam ring opening process [55]. The coordinating site offered by the host to the guest through keto group and the hydroxyl group is confirmed from the shifting of keto carbonyl IR peak of spirolactam ring at 1710 cm^{-1} to 1646 cm^{-1} and 1647cm^{-1} for **L**-Al^{3+} and **L**-Cr^{3+}, respectively (**Fig. S16, S17, and S18, ESI**). The lower wave no. of C=O and broadening of –OH band in IR spectra, which is practically due to the higher polarisation of these bond after induction with metal strongly supports the complexation of metal ion (Al^{3+}, and Cr^{3+}) with the ligand [56,57]. Disappearing of ^{13}C peaks at (δ) 66.03ppm (**Fig. S6, S7 ESI**) for sp^3 carbon and also disappearing of ^1H NMR peak at (δ) 10.92 ppm

(**Fig. S5, ESI**)for –OH proton along with shifting of –CH=N peak at (δ) 9.44 ppm supports the formation of **L**-Al^{3+} and **L**-Cr^{3+} complexation [58]. Again, the **L**-M^{n+} complexation as well as the better complexing ability of **L**-$Al^{3+}$is also be confirmed from the higher τ_{av} value of **L**-M^{n+} than bare **L** and higher τ_{av} value of **L**-Al^{3+} than **L**-Cr^{3+}complex (**Table-5**). Furthermore, the 1:1 binding pattern of the **L**-M^{n+} complex was confirmed from UV–Vis absorption by the Job's plot for **L** and M^{n+} (**Fig. S19, S20, S21 ESI**). A thorough inspection of the Job's plot exposed that absorption reaches its maxima near about 0.5-mole fraction of Cr^{3+} and Al^{3+} indicating ideal binding mode for **L**-Al^{3+} and **L**-Cr^{3+} complex, respectively. The superiority of our sensor **L** has been established by comparing the detection limit with many other reported probes **[Fig. S22 ESI**]

3.8 Logic gate interpretation

The quick and subtle response of our probes towards the dual metal inspired us to check its reversibility by constructing a double input and single output based noncommutative type logic gate [59,60]. The INHIBIT logic gate is constructed in the maximum emission of Al^{3+} and Cr^{3+} at λ_{em} = 582 nm and 581 nm with the basic theory of Boolean algebra where 1 represents 'YES'/'ON-state' and 0 pointing 'NO'/OFF-state. In the absence of both metal and EDTA, the output is zero indicating off state. In variation 2 when the input is only metal without EDTA maximum emission intensity is observed for Al^{3+} and Cr^{3+} at λ_{em} = 582 nm and 581 nm, respectively, pointing 1 (on) state, in the third row where EDTA is the only chemical entity to input,output is zero and in the fourth row where both the metals and EDTA is used as input, output again becomes zero. Therefore, input 1 performs the yes operation and the input 2 satisfies the criteria of NOT gate [61]. Considering all the results among the 16th TRUTH Table our truth table matches with the truth table of INHIBIT logic gate (**Fig. 10**).

(a)

Input 1(Al^{3+} or Cr^{3+})	Input 2 EDTA	Output (emission intensity 582/581nm)
0	0	0
1	0	1
0	1	0
1	1	0

(b)

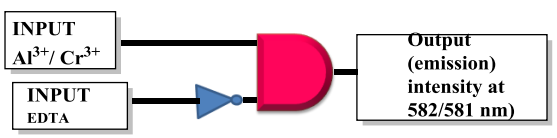

Fig. 10. (a) Truth table (b) circuit diagram for Inhibit Logic Gate

3.9 Geometry optimization and electronic structure

The optimized geometries of the Al^{3+} complex and its Cr^{3+} complex are shown in **Fig. 11**. The ground state geometry optimization for the complexes **1** and **2** were performed in the gas phase. Main optimized geometrical parameters of the complex **1** are listed in **Table 1** and for complex 2 in **Table 2**. In case of complex **1,** the Al^{3+} center is penta-coordinated with one di-deprotonated tridentate chelate $\mathbf{H_2L}$ ligand (with NO_2 donor sites) and one water molecule and one nitrate ion. The geometry of the penta-coordinated metal center is measured by the Addison parameter (τ), which is 0.006 for **1** in this case [$\tau = (\alpha - \beta)/60$, where α and β are the two largest Ligand-Metal-Ligand angles of the coordination sphere], suggesting a nearly square pyramidal geometry of around the Al^{3+} center ($\tau = 0$ for a perfect square pyramid and $\tau = 1$ for a perfect trigonal bi-pyramidal). The equatorial plane is occupied by one amide enol and one phenoxido oxygen (O1 and O2) and one immine Nitrogen (N1) and one water molecules (O1w), while the one axial site is occupied by an oxygen atom (O1n) of nitrate ion in **1**. In **1,** all calculated Al-N distances occur in the range 1.956Å and Al-O distances are in the range 1.908-1.929Å.

On the other hand for complex **2**, the metal center Cr^{3+} is being hexa-coordinated with one di-deprotonated tridentate chelate ligand (with NO_2 donor sites) and three water molecules to form a distorted octahedral geometry. The calculated Cr–N bond distance is 1.861Å and Cr–O bond distance are fall in the range 1.790-1.818Å.The equatorial sites are occupied by one amide enol and one phenoxido oxygen (O1 and O2) and one immine Nitrogen (N1) and oxygen (O3w) of the water molecule, while the axial sites are occupied by two aqua oxygens (O1w and O2w) in **2**.

In case of complex **1** at ground state, the electron density at HOMO, HOMO–1 and HOMO – 2 orbitals are mainly originating from ligand π and π* orbital contribution while the HOMO–3, LUMO and LUMO+1 orbitals arises from metal *d* orbital contribution along with ligand π orbital contribution. The energy difference between HOMO and LUMO is 0.878eV of ligand ($\mathbf{H_2L}$). In case of complex **2,** the electron density at HOMO, HOMO – 1, and HOMO – 2 orbitals are mainly resided on the benzene moiety and from metal *d* orbital contribution while a considerable contribution comes from p-nitro azo-benzene moiety along with the combination of rhodamine moiety in LUMO and LUMO+1 orbitals. The energy difference between HOMO and LUMO is 5.015eV of **2**.

The complex **1** shows a sharp absorption band at 554 nm in EtOH solution at room temperature. This experimental value was supported by the TDDFT calculation. This absorption band is assigned to the $S_0 \rightarrow S_{26}$ transition which is in good agreement with

experimental results of 547 nm. The absorption energies along with their oscillator strengths, the main configurations and their assignments calculated using TDDFT method using the ground state geometry for complex **1** is discussed here and the related data are given in **Table 3.**

The complex **2** exhibits one absorption band at 557 nm in ethanol solution at room temperature. The TDDFT calculated absorption band is located at 553 nm for **2**, which is in good agreement with the experimental results of 557 nm **(Table 4)**. This absorption band is assigned to the $S_0 \rightarrow S_{24}$ transition **(Table 4)**.

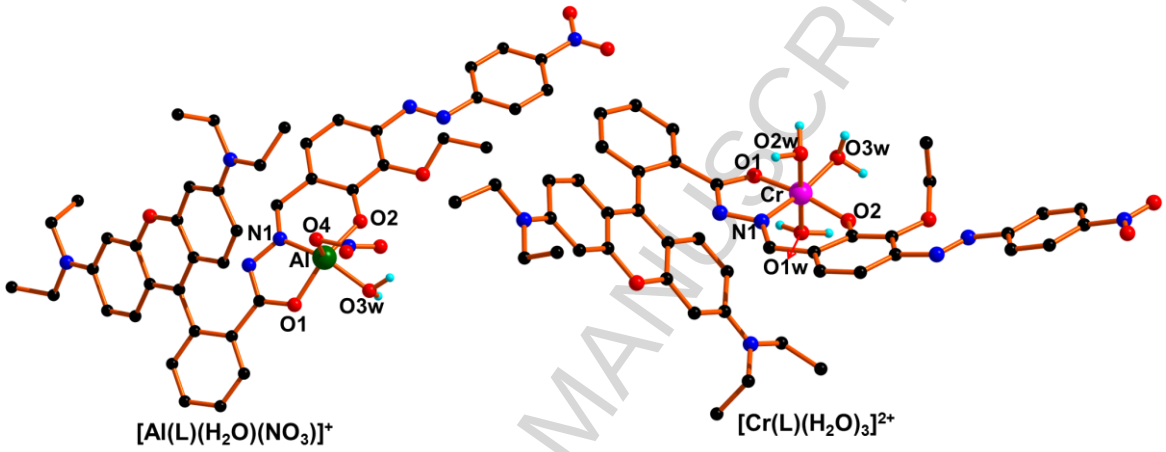

Fig. 11. DFT/B_3LYP optimized geometry of complexes $[Al(\mathbf{L})(H_2O)(NO_3)]^+$ (**1**) and as well as $[Cr(\mathbf{L})(H_2O)_3]^{2+}$(**2**).

Table 1: Selected optimized geometrical parameters for $[Al(\mathbf{L})(H_2O)(NO_3)]^+$ **(1)** in the ground state calculated at B_3LYP Levels.

Bonds	Values (Å)	Bond angles	Values (°)
Al1-N1	1.956	N1-Al1-O1	79.52
Al1-O1	1.918	O1-Al1-O2	147.50
Al1-O2	1.929	N1-Al1-O2	92.93
Al1-O1w	1.909	N1-Al1-O1n	106.24
Al1-O1n	1.908	N1- Al1-O1w	147.12
		O1- Al1-O1w	86.24
		O1- Al1-O1n	105.47

		O2- Al1-O1n	106.97
		O2- Al1-O1w	83.34
		O1a- Al1-O1m	88.75
		O1a- Al1-O1w	90.21
		O1a- Al1-O1n	90.07
		O1m- Al1-O1w	173.77
		O1m- Al1-O1n	84.92

Table 2: Selective bond distance and bond angles of $[Cr(\mathbf{L})(H_2O)_3]^{2+}$ (**2**).

Bonds	Values (Å)	Bond angles	Values (°)
Cr1-N1	1.861	N1-Cr1-O1	84.32
Cr1-O1	1.818	O1- Cr1-O2	163.35
Cr1-O2	1.806	N1- Cr1-O2	99.31
Cr1-O1w	1.806	N1- Cr1-O1w	84.57
Cr1-O2w	1.790	N1- Cr1-O2w	95.43
Cr1-O3w	1.800	N1- Cr1-O3w	167.81
		O1w- Cr1-O2w	179.97
		O1w- Cr1-O3w	83.27
		O1w- Cr1-O1	98.41
		O2- Cr1-O1w	98.07
		O2w- Cr1-O2	81.91
		O2w- Cr1-O1	81.52
		O2w- Cr1-O3w	96.70
		O3w- Cr1-O1	96.50
		O3w- Cr1-O2	83.39

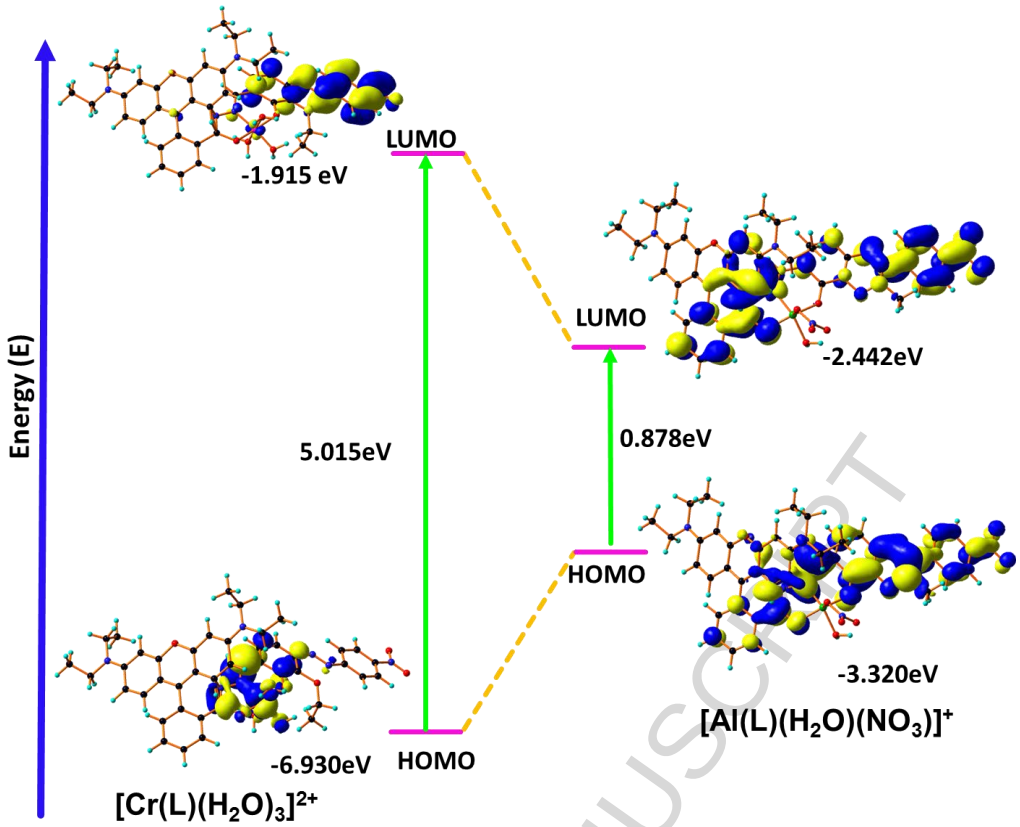

Fig. 12. Frontier molecular orbitals of optimized complexes.

Table 3: Selected parameters for the vertical excitation (UV-Vis absorptions) of complex **1** in terms of molecular orbital contribution of the transition; electronic excitation energies (eV) and oscillator strengths (*f*) in ethanol.

Electronic transition	Composition	Excitation energy	Oscillator strength (*f*)	CI	λ_{exp} (nm)
$S_0 \rightarrow S_{26}$	HOMO →LUMO + 1 HOMO – 2→ LUMO HOMO – 1→ LUMO +1	2.5414 eV (547nm)	0.0472	0.66278 0.63547 0.28628	554

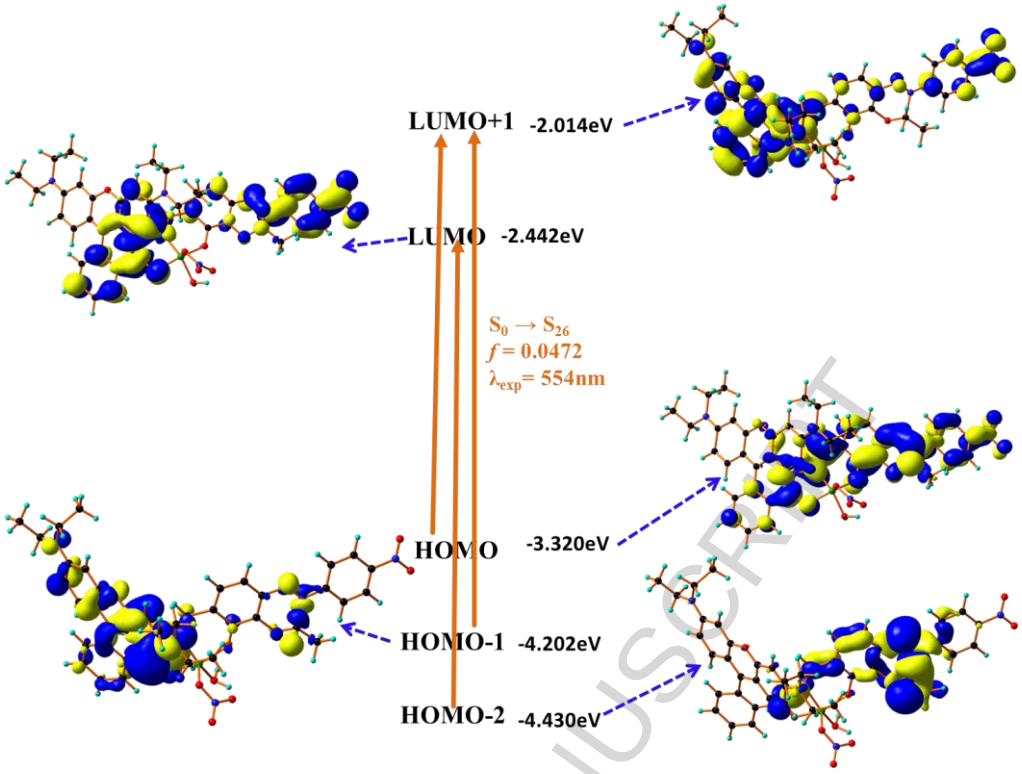

Fig. 13. Frontier molecular orbitals involved in the UV-Vis absorption of complex **1**.

Table 4: Main calculated optical transition for the complex **2** with the composition in terms of molecular orbital contribution of the transition, vertical excitation energies, and oscillator strength in ethanol.

Electronic transition	Composition	Excitation energy	Oscillator strength (*f*)	CI	λ_{exp} (nm)
$S_0 \rightarrow S_{24}$	HOMO – 1 →LUMO HOMO →LUMO HOMO – 2 →LUMO +1	2.3627 eV (553 nm)	0.0309	0.58251 0.27015 0.45910	557

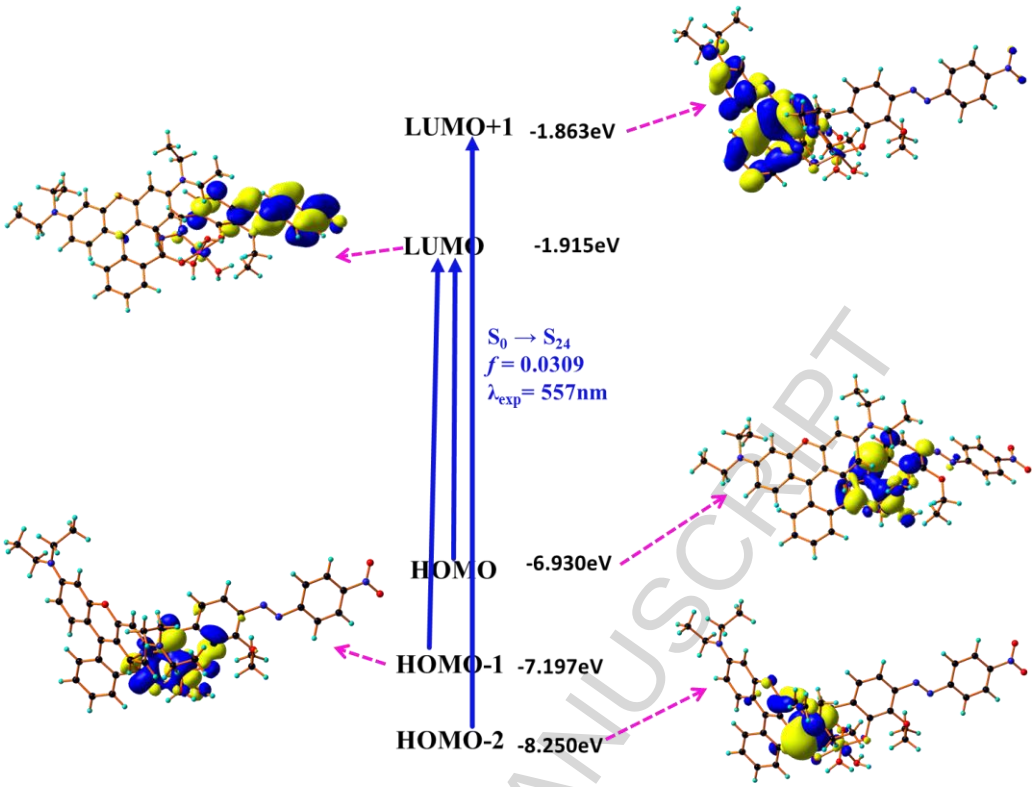

Fig. 14. Frontier molecular orbitals involved in the UV-Vis absorption of complex **2**.

3.10 Time-Correlated Single Photon Counting (TCSPC) Study

The enhancement of fluorescence of **L** upon binding with Al^{3+} and Cr^{3+}has been supported by the results obtained from fluorescence decay measurements, using the TCSPC technique (**Fig. 15**). The decay behavior of the bare probe and its metal complex is best fitted to bi-exponential functions. Bare **L** showed two components having lifetimes 0.13 and 2.34 ns respectively. The populations of the same were 0.94 and 0.06 % respectively. The average lifetime of **L** was calculated to be 0.54 ns. Upon addition of Al^{3+}, two components were obtained having lifetimes 0.38 and 1.89 ns respectively, having populations of 0.78 and 0.22 % respectively (**Table 5**). The average lifetime was calculated to be 1.31 ns. A similar experiment performed with comparable Cr^{3+} showed a bi-exponential decay trace with time constants τ_1 = 0.36 (0.77 %) and τ_2 = 1.72 (0.23 %). The average lifetime was calculated to be 1.19 ns. Upon binding of Al^{3+} and Cr^{3+} to the (**L**) formation of a tight binding complex occurs along with the opening of the spirolactam ring to convert the free (hanging) Rhodamine B part of the complex, thereby freezing of non-radiative pathways generated by

rigid structure of the complex than the comparatively more flexible structure of the bare ligand.[62]As a result the average lifetime increased.

Table 5: Fluorescence lifetimes of **L**, **L-Al^{3+}** and **L-Cr^{3+}** complexes in EtOH-H_2O solvent

EtOH/H_2O	τ_1(ns)	τ_2(ns)	α_1	α_2	χ^2	τ_{av}
L	0.13	2.34	0.94	0.06	1.07318	0.54
L-Al^{3+}	0.38	1.89	0.78	0.22	0.99236	1.31
L-Cr^{3+}	0.36	1.72	0.77	0.23	0.995	1.19

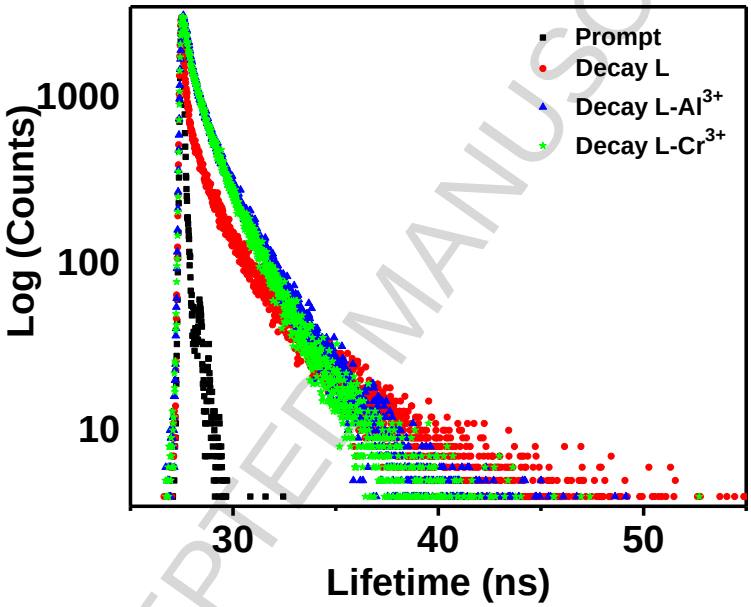

Fig. 15. Life-time measurements of **L** , **L**–Al^{3+} and **L**–Cr^{3+}(λ_{ex} = 520 nm)

3.11 Cell imaging study

The overnight sub-confluent culture of human lymphocyte cells (HLC) was washed with phosphate buffer saline (PBS; pH 7.4) and incubated with DMEM containing **L** with the final concentration at 5 µM for 3h at 37 °C in CO_2 incubator. After incubation, fluorescence images of HLCs were captured under a fluorescence microscope (LEICA DFC295, Germany) in 40X magnification. Similarly, a fluorescence image of HLCs (pre-incubated with 5 µML) was taken after addition of Al^{3+} and Cr^{3+} salt solution at the concentration of 10 µM for 1h separately with an excitation wavelength 582 and 581 nm [63].

3.11.1 *In vitro* cell cytotoxicity

To reproduce the capability of the fluorescence-based probe for intracellular imaging of Al^{3+} and Cr^{3+}, firstly, it was of prime importance to verify the cytotoxic effect of the ligand on normal human cells. To establish the biocompatibility of the ligand in the cellular environment, the performed cell viability study by standard MTT assay in human lymphocyte cells (HLCs) revealed that 93.6 ± 0.54 % cell viability was observed at the concentration of 5 µM in the presence of **L** compared to HLC-control cells. The viability of the cells has been observed in a dose-dependent manner up to the concentration of 100 µM. Ligand showed 45.3 ± 0.48 % cytotoxicity at 100 µM concentration after 24 h incubation, whereas only 6.2 + 0.51 % cytotoxicity at 5 µM concentration at the same incubation time. It has been assumed that ligand did not influence the viability of HLCs at least 24h of its treatment at concentration 5 µM (**Fig. 16**).

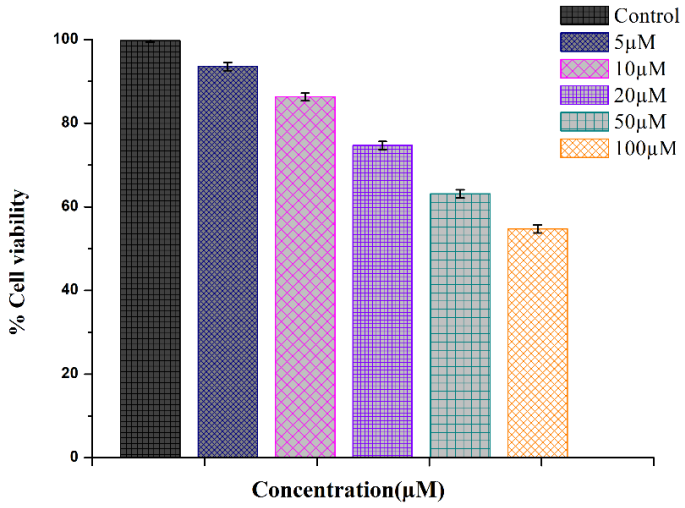

Fig. 16. % cells viability study of HLCs treated with different concentration (5-100 µM) of Ligand for 24h by MTT assay. Values are expressed as the mean ± S.D. of three independent experiments.

3.11. 2 Fluorescence cell imaging study

No intracellular fluorescence was observed in a fluorescence cell imaging study, after the incubation with the ligand at a concentration of 5 µM at 37 °C for 1h. However, intensive intracellular green switch-on fluorescence is observed after the incubation with exogenous Al^{3+} ion (10 µM) and Cr^{3+} (10 µM) solution and the fluorescence intensity of **L**-Al^{3+} is quite higher than the **L**-Cr^{3+} salt solution (**Fig. 17**). The fluorescence image of the **L** with Al^{3+} and

Cr^{3+} salt offers the confirmatory evidence that the **L** easily infiltrates the cell membrane and bind with intracellular Al^{3+} and Cr^{3+} forming the **L**-Al^{3+} and **L**-Cr^{3+}complex respectively. The present study proposes that **L** could be utilized as an ineffaceable signature of the selective sensor for bio-imaging Al^{3+} ions at the specified doses and incubation time without showing any cytotoxic effect.

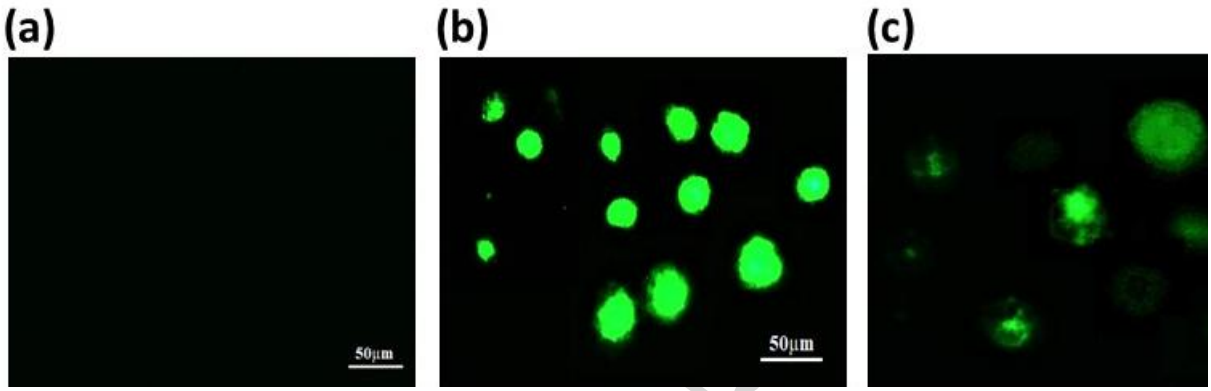

Fig. 17. (a) Fluorescence image of HLCs incubated with Ligand (5μM), (b) Al^{3+} salt solution (10μM), and (c) Cr^{3+} salt solution (10 μM).

4. Conclusion

In summary, we have demonstrated an inexpensive, solvatochromic–based highly efficient, fast turn-on probe, **L**. The **L** in its stable metal-induced conjugated chelated form expresses its strong off-on selectivity response towards Al^{3+}, Cr^{3+}, and Cu^{2+} detected by UV-Visible absorption whereas Al^{3+} and Cr^{3+} detected by fluorimetric study. Larger association constants 6.7435×10^{3} M^{-1}, 3.8×10^{3} M^{-1}, and 5.685×10^{3} M^{-1} for Al^{3+}, $Cr^{3+,}$ and Cu^{2+}, respectively and nanomolar limit of detection 1.07×10^{-6} M, 2.02×10^{-6} M, 1.6×10^{-6} M for Al^{3+}, Cr^{3+}, and Cu^{2+}, respectively along with insignificant interference from the common co-existing metal ions makes **L** as a convenient tool for effective detection Al^{3+}, $Cr^{3+,}$ and Cu^{2+}. Our work is the first to report on Cr^{3+} chemosensor based on rhodamine-azobenzene moiety. We have also constructed INHIBIT molecular Logic gate using the sensing properties. High sustainability in physiological pH and high-resolution cell imaging experiment in human lymphocyte cell further confirmed its applicability without toxicity in living biological system for monitoring the intercellular level of Al^{3+} and Cr^{3+}. We hope our rhodamine-azobenzene based chemosensor will open up new possibilities for synthesizing cost-effective dual analyte recognizing sensor in recent future.

Conflicts of interest

There is no conflict of interest to declare.

Acknowledgments

S. Dey thanks University Grants Commission, New Delhi, India, for financial support by sanctioning a Minor Research Project (Sanction Letter No. PSW-155/14-15(ERO) ID No. WV6-027, S. No. 223832 dated 03-2015). We thank Dr. Asim Kr. Bera, Principal, Mahisadal Raj College and Dr. Sujit Kr. Bera, Teacher-in-charge, Tamralipta Mahavidyalaya for providing laboratory and instrumental facilities.

References

[1] J. Li, C. Han, W. Wu, S. Zhang, J. Guo, H. Zhou, R. Kagit, M. Yildirim, O. Ozay, S. Yesilot, H. Ozay, X. Wu, Z. Guo, Y. Wu, S. Zhu, T.D. James, W. Zhu, Phosphazene based multicentered naked-eye fluorescent sensor with high selectivity for Fe^{3+}ions, Inorg. Chem. 53 (2014) 2144–2151.

[2] J. Li, C. Han, W. Wu, S. Zhang, J. Guo, H. Zhou, Selective and cyclic detection of Cr^{3+}using poly(methylacrylic acid) monolayer protected gold nanoparticles, New J. Chem. 38 (2014) 717–722.

[3] X. Wu, Z. Guo, Y. Wu, S. Zhu, T.D. James, W. Zhu, Near-infrared colorimetric and fluorescent Cu^{2+} sensors based on indoline-benzothiadiazole derivatives via formation of radical cations, ACS Appl. Mater. Interfaces. 5 (2013) 12215–12220.

[4] L. Huang, F. Chen, P. Xi, G. Xie, Z. Li, Y. Shi, M. Xu, H. Liu, Z. Ma, D. Bai, Z. Zeng, A turn-on fluorescent chemosensor for Cu^{2+}in aqueous media and its application to bioimaging, Dye. Pigment. 90 (2011) 265–268.

[5] L. Hou, X. Kong, Y. Wang, J. Chao, C. Li, C. Dong, Y. Wang, S. Shuang, An anthraquinone-based highly selective colorimetric and fluorometric sensor for sequential detection of $Cu^{2+}$and S^{2-} with intracellular application, J. Mater. Chem. B. 5 (2017) 8957–8966.

[6] F. Yu, W. Zhang, P. Li, Y. Xing, L. Tong, J. Ma, B. Tang, Cu^{2+}-selective naked-eye and fluorescent probe: Its crystal structure and application in bioimaging, Analyst. 134 (2009) 1826–1833.

[7] D. Zhu, A. Ren, X. He, Y. Luo, Z. Duan, X. Yan, Y. Xiong, X. Zhong, A novel ratiometric fluorescent probe for selective and sensitive detection of Cu^{2+}in complete aqueous solution, Sensors Actuators, B Chem. 252 (2017) 134–141.

[8] P. Mahato, S. Saha, E. Suresh, R. Di Liddo, P.P. Parnigotto, M.T. Conconi, M.K. Kesharwani, B. Ganguly, A. Das, Ratiometric detection of Cr^{3+} and Hg^{2+} by a naphthalimide-rhodamine based fluorescent probe., Inorg. Chem. 51 (2012) 1769–77.

[9] A.K. Bhanja, S. Mishra, K. Naskar, S. Maity, K. Das Saha, C. Sinha, Specific recognition of Cr^{3+} under physiological conditions by allyl substituted appendage rhodamine and its cell-imaging studies, Dalt. Trans. 46 (2017) 16516–16524.

[10] X. li Yue, Z. qing Wang, C. rui Li, Z. yin Yang, Naphthalene-derived Al^{3+}-selective fluorescent chemosensor based on PET and ESIPT in aqueous solution, Tetrahedron Lett. 58 (2017) 4532–4537.

[11] L. Tang, F. Li, M. Liu, R. Nandhakumar, Spectrochimica Acta Part A : Molecular and Biomolecular Spectroscopy Single sensor for two metal ions : Colorimetric recognition of Cu^{2+} and fluorescent recognition of Hg^{2+}, Spectrochim. Acta Part A Mol. Biomol. Spectrosc. 78 (2011) 1168–1172.

[12] X. Yu, H. Qu, Q. Hu, K. Hou, Y. Yan, D. Wu, P. Zhang, J. Li, A rhodamine-based sensor for chromogenic detection of Cu^{2+} and fluorescent detection of Fe^{3+}, Wuhan Univ. J. Nat. Sci. 19 (2014) 129–136.

[13] N. Singh, N. Kaur, C. Ni Choitir, J.F. Callan, A dual detecting polymeric sensor: chromogenic naked eye detection of silver and ratiometric fluorescent detection of manganese, Tetrahedron Lett. 50 (2009) 4201–4204.

[14] D.Y. Lee, N. Singh, D.O. Jang, A benzimidazole-based single molecular multianalyte fluorescent probe for the simultaneous analysis of Cu^{2+} and Fe^{3+}, Tetrahedron Lett. 51 (2010) 1103–1106.

[15] P. Kaur, D. Sareen, The synthesis and development of a dual-analyte colorimetric sensor: Simultaneous estimation of $Hg^{2+}$and Fe^{3+}, Dye. Pigment. 88 (2011) 296–300.

[16] S.G. and A.M. Sima Paul, A differentially selective molecular probe for detection of trivalent ions (Al^{3+}, Cr^{3+} and Fe^{3+}) upon single excitation in mixed aqueous medium, Dalt. Trans. 44 (2015) 11805–11810.

[17] Ajit Kumar Mahapatra, Saikat Kumar Manna, Kalipada Maiti, Sanchita Mondal, Rajkishor Maji, Debasish Mandal, Sukhendu Mandal, Md. Raihan Uddin, Shyamaprosad Goswami, Ching Kheng Quah and Hoong-Kun Fun Azodye−Rhodamine-Based Fluorescent and Colorimetric Probe Specific for the

Detection of Pd^{2+} in Aqueous Ethanolic Solution: Synthesis, XRD characterization, Computational Studies and Imaging in Live Cells, Analyst. 140 (2015) 1229–1236.

[18] Ha Na Kim, Seong-Won Nam, K. M. K. Swamy, Yan Jin, Xiaoqiang Chen, Yonugmee Kim . Sung-Jin Kim, Sungsu Park and Juyoung Yoon Rhodamine hydrazone derivatives as Hg^{2+} selective fluorescent and colorimetric chemosensors and their applications to bioimaging and microfluidic system, Analyst. 136 (2011) 1339 – 1343.

[19] M. Dolai, U. Saha, A.K. Das, G. Suresh Kumar, Single sensors for multiple analytes employing fluorometric differentiation for $Cr^{3+}$and Al^{3+}in semi-aqueous medium with bio-activity and theoretical aspects, Anal. Methods. 10 (2018) 4063–4072.

[20] 1. L. Hudson and F. C. Hay, Practical immunology, Blackwell Pub,Oxford. (1989).

[21] T. Mosmann, Rapid colorimetric assay for cellular growth and cytotoxicity assays., J Immunol Methods. 65 (1983) 55–63.

[22] R. G. Parr and W. Yang, Density Functional Theory of Atoms and Moleculesle, Oxford University Press, Oxford, 1989.

[23] M. Cossi, N. Rega, G. Scalmani, V. Barone, D. Chimica, F. Ii, C.M.S. Angelo, CPCM-Molecules in Solution with the C-PCM Solvation Model, J. Com. 24 (2003) 669–681.

[24] M. Cossi, V. Barone, Time-dependent density functional theory for molecules in liquid solutions, J. Chem. Phys. 115 (2001) 4708–4717.

[25] V. Barone, M. Cossi, Conductor Solvent Model, J. Phys. Chem. A. 102 (1998) 1995–2001.

[26] A.D. Becke, Development of the Colic-Salvetti correlation-energy formula into a functional of the electron density, J. Chem. Phys. 98 (1993) 5648–5652.

[27] C. Lee, C. Hill, N. Carolina, Development of the Colle-Salvetti correlation-energy formula into a functional of the electron density, Phys. Rev. B. 37 (1988) 785–789.

[28] R.E. Stratmann, G.E. Scuseria, M.J. Frisch, An efficient implementation of time-dependent density-functional theory for the calculation of excitation energies of large molecules, J. Chem. Phys. 109 (1998) 8218.

[29] M.E. Casida, C. Jamorski, K.C. Casida, D.R. Salahub, Molecular excitation energies to high-lying bound states from time-dependent density-functional response theory: Characterization and correction of the time-dependent local density approximation ionization threshold, J. Chem. Phys. 108 (1998) 4439–4449.

[30] R. Ahlrichs, R. Bauernschmitt, Treatment of electronic excitations within the adiabatic approximation of time dependent density functional theory, Chem. Phys. Lett. 256

(1996) 454–464.

[31] X. Zhou, A.M. Ren, J.K. Feng, Theoretical studies on the ground states in M(terpyridine)$^{22+}$ and M(n-butyl-phenylterpyridine)$^{22+}$ (M = Fe, Ru, Os) and excited states in Ru(terpyridine)$^{22+}$ using density functional theory, J. Organomet. Chem. 690 (2005) 338–347.

[32] T. Liu, H.-X. Zhang, B.-H. Xia, Theoretical Studies on Structures and Spectroscopic Properties of a Series of Novel Cationic [*trans* -(C ^ N) $_2$ Ir(PH $_3$) $_2$] $^+$ (C ^ N = ppy, bzq, ppz, dfppy), J. Phys. Chem. A. 111 (2007) 8724–8730.

[33] B.-H.X. and A.T. Zhou Xin, Hong-Xing Zhang, Qing-Jiang Pan, Theoretical Studies of the Spectroscopic Properties of [Pt (trpy) C t CR] $^+$ (trpy), 109 (2005) 8809–8818.

[34] J.C. and D.J.F. M. J. Frisch, G. W. Trucks, H. B. Schlegel, G. E. Scuseria, M. A. Robb, J. R. Cheeseman, G. Scalmani, V. Barone, B. Mennucci, G. A. Petersson, H. Nakatsuji, M. Caricato, X. Li, H. P. Hratchian, A. F. Izmaylov, J. Bloino, G. Zheng, J. L. Sonnenberg, M. Had, Gaussian 09, (Revision A.1), (2009).

[35] S. Hashmi, S.A. Salam, Acute myocardial infarction and myocardial ischemia-reperfusion injury: A comparison, Int. J. Clin. Exp. Pathol. 29 (2008) 839–845.

[36] J.R. Lakowicz, Principles of Fluorescence Spectroscopy, Plenum, New York. (1999).

[37] B. Ramachandram, G. Saroja, B. Sankaran, A. Samanta, Unusually High Fluorescence Enhancement of Some 1,8-Naphthalimide Derivatives Induced by Transition Metal Salts, J. Phys. Chem. B. 104 (2000) 11824–11832.

[38] S. Banthia, A. Samanta, A new strategy for ratiometric fluorescence detection of transition metal ions, J. Phys. Chem. B. 110 (2006) 6437–6440.

[39] S. Mabhai, M. Dolai, S. Dey, A. Dhara, B. Das, A. Jana, A novel chemosensor based on rhodamine and azobenzene moieties for selective detection of Al^{3+} ions, New J. Chem. 42 (2018) 10191–10201.

[40] M.S. Bashandy, F.A. Mohamed, M.M. El-Molla, M.B. Sheier, A.H. Bedair, Synthesis of Novel Acid Dyes with Coumarin Moiety and Their Utilization for Dyeing Wool and Silk Fabrics, Open J. Med. Chem. 6 (2016) 18–35.

[41] H.A. Benesi, J.H. Hildebrand, A Spectrophotometric Investigation of the Interaction of Iodine with Aromatic Hydrocarbons, J. Am. Chem. Soc. 71 (1949) 2703–2707.

[42] L.-Q. Yan, M.-F. Cui, Y. Zhou, Y. Ma, Z.-J. Qi, A Simplified and turn-on fluorescence chemosensor based on coumarin derivative for detection of aluminium(III) ion in pure aqueous solution, Anal. Sci. 31 (2015) 1055–1059.

[43] D. Maity, T. Govindaraju, Conformationally constrained (Coumarin-Triazolyl-Bipyridyl) click fluoroionophore as a selective Al^{3+} sensor, Inorg. Chem. 49 (2010) 7229–7231.

[44] A. Dhara, A. Jana, N. Guchhait, P. Ghosh, S.K. Kar, Rhodamine-based molecular clips for highly selective recognition of Al^{3+} ions: Synthesis, crystal structure and spectroscopic properties, New J. Chem. 38 (2014) 1627–1634.

[45] Z.Y. Bing-jie Pang, Chao-rui Li, Design of a colorimetric and turn-on fluorescent probe for the detection of Al(III), J. Photochem. Photobiol. A Chem. 356 (2018) 159–165.

[46] X. Tang, J. Han, Y. Wang, L. Ni, X. Bao, L. Wang, W. Zhang, A multifunctional Schiff base as a fluorescence sensor for Fe^{3+} and Zn^{2+} ions, and a colorimetric sensor for Cu^{2+} and applications, Spectrochim. Acta - Part A Mol. Biomol. Spectrosc. 173 (2017) 721–726.

[47] S. Mabhai, A. Jana, S. Dey, A novel rhodamine-based colorimetric and fluorometric chemosensor for selective detection of Al^{3+} ion in CH_3CN-H_2O solution, J. Indian Chem. Soc., 92 (2015) 1–10.

[48] A. Jana, B. Das, S.K. Mandal, S. Mabhai, A.R. Khuda-Bukhsh, S. Dey, Deciphering the CHEF-PET-ESIPT liaison mechanism in a Zn^{2+}chemosensor and its applications in cell imaging study, New J. Chem. 40 (2016) 5976–5984.

[49] B. jie Pang, C. rui Li, Z. yin Yang, Design of a colorimetric and turn-on fluorescent probe for the detection of Al(III), J. Photochem. Photobiol. A Chem. 356 (2018) 159–165.

[50] I.H. Hwang, Y.W. Choi, K.B. Kim, G.J. Park, J.J. Lee, L. Nguyen, I. Noh, C. Kim, A highly selective and sensitive fluorescent turn-on Al^{3+} chemosensor in aqueous media and living cells: experimental and theoretical studies, New J. Chem. 40 (2016) 171–178.

[51] Jeong Ho Chang, Young Muk Choi, Y.K. Shin, A significant fluorescence quenching of anthrylaminobenzocrown ethers by paramagnetic metal cations, Bull. Korean Chem. Soc. 22 (2001) 527–530.

[52] O. Sunnapu, N.G. Kotla, B. Maddiboyina, G.S. Asthana, J. Shanmugapriya, K. Sekar, S. Singaravadivel, G. Sivaraman, Rhodamine based effective chemosensor for Chromium(III) and their application in live cell imaging, Sensors Actuators, B Chem. 246 (2017) 761–768.

[53] S. Sahana, G. Mishra, S. Sivakumar, P.K. Bharadwaj, Rhodamine – Cyclohexane

diamine based "turn-on" fluorescence chemosensor for Cr^{3+}: Photophysical & confocal cell imaging studies, J. Photochem. Photobiol. A Chem. 351 (2018) 42–49.

[54] A. Sahana, A. Banerjee, S. Lohar, B. Sarkar, S.K. Mukhopadhyay, D. Das, Rhodamine-based fluorescent probe for Al^{3+} through time-dependent PET-CHEF-FRET processes and its cell staining application, Inorg. Chem. 52 (2013) 3627–3633.

[55] X. Tang, J. Han, Y. Wang, L. Ni, X. Bao, L. Wang, W. Zhang, A multifunctional Schiff base as a fluorescence sensor for Fe^{3+} and Zn^{2+} ions, and a colorimetric sensor for Cu^{2+} and applications, Spectrochim. Acta - Part A Mol. Biomol. Spectrosc. 173 (2017) 721–726.

[56] T. Mistri, R. Alam, M. Dolai, S. Kumar Mandal, P. Guha, A. Rahman Khuda-Bukhsh, M. Ali, Rhodamine-based chromo-/fluorogenic dual signalling probe for selective recognition of HgIIwith potential applications for INHIBIT logic devices and cell-imaging studies, Eur. J. Inorg. Chem. (2013) 5854–5861.

[57] P. Mahato, S. Saha, E. Suresh, R. Di Liddo, P.P. Parnigotto, M.T. Conconi, M.K. Kesharwani, B. Ganguly, A. Das, Ratiometric detection of $Cr^{3+}$and Hg^{2+} by a naphthalimide-rhodamine based fluorescent probe, Inorg. Chem. 51 (2012) 1769–1777.

[58] K. Ghosh, T. Sarkar, A. Samadder, A rhodamine appended tripodal receptor as a ratiometric probe for Hg^{2+} ions, Org. Biomol. Chem. 10 (2012) 3236–3243.

[59] S. Dey, S. Sarkar, D. Maity, P. Roy, Rhodamine based chemosensor for trivalent cations: Synthesis, spectral properties, secondary complex as sensor for arsenate and molecular logic gates, Sensors Actuators, B Chem. 246 (2017) 518–534.

[60] T. Gunnlaugsson, D.A. Mac Dónall, D. Parker, Luminescent molecular logic gates: The two-input inhibit (INH) function, Chem. Commun. (2000) 93–94.

[61] C.B. Bai, R. Qiao, J.X. Liao, W.Z. Xiong, J. Zhang, S.S. Chen, S. Yang, A highly selective and reversible fluorescence "OFF-ON-OFF" chemosensor for Hg^{2+} based on rhodamine-6G dyes derivative and its application as a molecular logic gate, Spectrochim. Acta - Part A Mol. Biomol. Spectrosc. 202 (2018) 252–259.

[62] A. Dhara, A. Jana, S.K. Mandal, A.R. Khuda-Bukhsh, N. Guchhait, S.K. Kar, A unique rhodamine-based "off-on" molecular spy for selective detection of trivalent aluminum and chromium ions: Synthesis, crystal structure and spectroscopic properties along with living cell imaging, Inorganica Chim. Acta. 423 (2014) 454–461.

[63] A. Pradhan, M. Bepari, P. Maity, S.S. Roy, S. Roy, S.M. Choudhury, Gold nanoparticles from indole-3-carbinol exhibit cytotoxic, genotoxic and antineoplastic

effects through the induction of apoptosis, RSC Adv. 6 (2016) 56435–56449.

Graphical Abstract

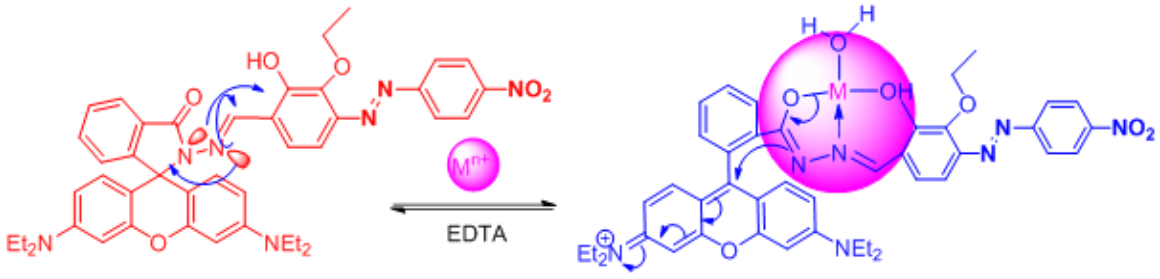

HIGHLIGHTS

- A new rhodamine-azobenzene based chemosensor was reported.
- Al^{3+}, Cr^{3+} , and and Cu^{2+} were detected by UV-Visible absorption study.
- Cr^{3+} and Al^{3+} were distinguished by fluorimetric study.
- The 1:1 on binding phenomenon of **L** and M^{n+} was confirmed by Job's plot.
- An INHIBIT LOGIC GATE is constructed at molecular level.
- The **L** was utilized to map the intracellular concentration of Al^{3+} or Cr^{3+} in HLCs.